

# Kinematics of shot-geophone migration

*Christiaan C. Stolk* \*, *Maarten V. de Hoop* †, *William W. Symes* ‡

## ABSTRACT

In contrast to prestack migration methods based on data binning, common image gathers produced by shot-geophone migration exhibit the appropriate semblance property in either offset domain (focussing at zero offset) or angle domain (focussing at zero slope), when the migration velocity is kinematically correct and when events to be migrated arrive in the data along non-turning rays. The latter condition is required for successful implementation via wavefield depth extrapolation. Thus shot-geophone migration may be a particularly appropriate tool for migration velocity analysis of data exhibiting structural complexity.

## INTRODUCTION

The basis of migration velocity analysis is the *semblance principle*: prestack migrated data volumes contain *flat image gathers*, i.e. are at least kinematically independent of the bin or stacking parameter, when the velocity is correct (Kleyn, 1983; Yilmaz, 1987). Migration velocity analysis (as opposed to standard NMO-based velocity analysis) is most urgently needed in areas of strong lateral velocity variation, i.e. “complex” structure such as salt flanks, chalk tectonics, and overthrust geology. However strong refraction implies multiple raypaths connecting source and receiver locations with reflection points, and multiple raypaths in turn imply that the semblance principle is not valid: that is, image

---

\*Department of Applied Mathematics, University of Twente, Drienerlolaan 5, 7522 NB Enschede, The Netherlands, email [c.c.stolk@ewi.utwente.nl](mailto:c.c.stolk@ewi.utwente.nl)

†Center for Wave Phenomena, Colorado School of Mines, Golden, CO 80110 USA, email [dehoop@mines.edu](mailto:dehoop@mines.edu)

‡The Rice Inversion Project, Department of Computational and Applied Mathematics, Rice University, Houston TX 77251-1892 USA, email [symes@caam.rice.edu](mailto:symes@caam.rice.edu)

gathers are *not* in general flat, even when the migration velocity closely approximates the true propagation velocity (Stolk and Symes, 2004).

The failure of the semblance principle in complex structure afflicts all prestack migration techniques based on data binning, i.e. for which each data bin creates an independent image. This category includes many variants of common shot, common offset and common scattering angle migration (Nolan and Symes, 1996; Nolan and Symes, 1997; Xu et al., 2001; Brandsberg-Dahl et al., 2003; Stolk, 2002; Stolk and Symes, 2004).

However one well-known form of prestack image formation does *not* migrate image bins independently: this is Claerbout’s *survey-sinking migration*, or *shot-geophone migration* (Claerbout, 1971; Claerbout, 1985), commonly implemented using some variety of one-way wave equation to extrapolate source and receiver depths. Such depth extrapolation implementation presumes that rays carrying significant energy travel essentially vertically (dubbed the “DSR condition” by Stolk and De Hoop (2001)). Source and receiver wavefields may be extrapolated separately, and correlated at each depth (shot profile migration), or simultaneously (DSR migration). In either case, the prestack migration output at each image point depends on a range of sources and receivers, not on data from a single bin defined by fixing any combination of acquisition parameters.

This paper demonstrates that a semblance principle appropriate for shot-geophone migration holds *regardless of velocity field complexity*, assuming

- the DSR condition,
- enough data to determine wavefield kinematics (for example, areal or “true 3D” acquisition in general, or narrow azimuth data plus mild cross-line heterogeneity), and
- a kinematically correct migration velocity field.

This result was established by Stolk and De Hoop (2001). We give a somewhat simpler derivation of this property, and a number of 2D illustrations. This semblance principle takes several roughly equivalent forms, corresponding to several available methods for forming image gathers. Sherwood and Schultz (1982), Claerbout (1985), and others defined image gathers depending on (subsurface) offset and depth: in such *offset image*

*gathers*, energy is *focussed* at zero offset when the velocity is kinematically correct. De Bruin et al. (1990) and Prucha et al (1999) gave one definition of *angle image gathers*, while Sava and Fomel (2003) suggest another. Such gathers are functions of scattering angle and depth. In both cases, correct migration velocity focusses energy at *zero slope*, i.e. angle image gathers are flattened at correct migration velocity.

As a by-product of our analysis, we observe that the semblance principle is a result of the mathematical structure of shot-geophone migration, not of any particular approach to its implementation. In particular, it is not depth extrapolation *per se* that is at the root of the favorable kinematic properties stated in the last paragraph. Indeed, a shot-geophone variant of two-way reverse time migration (Biondi and Shan, 2002; Symes, 2002) implements the same kinematics hence conforms to the same semblance principle. This two-way variant does not require the DSR assumption, and may employ nonhorizontal offsets. It is even possible to write a “Kirchhoff” formula for shot-geophone migration, which also satisfies the semblance principle.

To emphasize the main assertion of this paper: all versions (angle, offset) of the semblance principle for shot-geophone migration hold regardless of degree of multipathing and of computational implementation, provided that the assumptions stated above are valid. In particular, angle imaging via shot-geophone migration, using either method of angle gather formation mentioned above, is *not* equivalent, even kinematically, to Kirchhoff common angle imaging (Xu et al., 2001; Brandsberg-Dahl et al., 2003) - indeed, the latter typically generates kinematic artifacts when multiple ray paths carry important energy.

The “enough data” condition listed second above is quite as important as the others, as will be explained below. For arbitrary 3D complexity in the migration velocity field, validity of the semblance principle requires areal coverage (“true 3D” data). In particular we cannot guarantee the absence of kinematic artifacts in shot-geophone migration of narrow azimuth data, unless the velocity model is assumed to have additional properties, for example mild cross-line heterogeneity, which compensate to some extent for the lack of azimuths. This issue will be discussed a bit more in the concluding section.

Sherwood and Schultz (1982) observed that the focussing property of shot-geophone migration might serve as the basis for an approach to velocity estimation. Its freedom from

artifacts suggests that shot-geophone migration may be a particularly appropriate tool for migration velocity analysis of data acquired over complex structures. Some preliminary investigations of this idea have been carried out by Shen et al. (2003).

The paper begins with a very general description of shot-geophone migration operator as adjoint to an *extended* Born (single-scattering) modeling operator. All prestack migration methods, including those based on data binning, can be described in this way, as adjoint to extended modeling of some sort. The basic kinematics of shot-geophone prestack migration then follow easily from the high-frequency asymptotics of wave propagation. We summarize these kinematic properties, and present the outline of a complete derivation in the Appendix.

When offsets are restricted to be horizontal, as was the case in the original formulation of shot-geophone migration (Claerbout, 1985; Schultz and Sherwood, 1982), and the DSR condition is assumed, the artifact-free result of Stolk and De Hoop (2001) follows easily from the general kinematic properties already described, for both offset image gathers and angle image gathers in the style of Sava and Fomel (2003). We also review an alternative construction of angle image gathers due to De Bruin et al. (1990). We show how the semblance property for this form of angle domain migration follows from the general properties of shot-geophone migration.

Finally we present a number of examples illustrating the semblance property, using 2D synthetic data of increasing ray path complexity. Each example contrasts the angle image gathers produced by (Kirchhoff or Generalized Radon Transform) common scattering angle migration (Xu et al., 2001; Brandsberg-Dahl et al., 2003) with those produced by shot-geophone migration. In each case, kinematic artifacts appear in the former but not the latter. We use a one-way method (DSR migration implemented with a generalized screen propagator) to construct the shot-geophone migrations presented here.

## SHOT-GEOPHONE MIGRATION AS ADJOINT OF EXTENDED BORN MODELING

We assume that sources and receivers lie on the same depth plane, and adjust the depth axis so that the source-receiver plane is  $z = 0$ . This restriction can be removed at the cost of more complicated notation (and numerics): it is not essential. Nothing about

the formulation of the migration method presented below *requires* that data be given on the full surface  $z = 0$ .

While the examples to be presented later are all 2D, the construction is not: in the following  $\mathbf{x}$  (and other bold face letters) will denote either two- or three-dimensional vectors. Source locations are  $\mathbf{x}_s$ , receiver locations are  $\mathbf{x}_r$ .

### Single scattering

The causal acoustic Green's function  $G(\mathbf{x}, t; \mathbf{x}_s)$  for a point source at  $\mathbf{x} = \mathbf{x}_s$  is the solution of

$$\frac{1}{v^2(\mathbf{x})} \frac{\partial^2 G}{\partial t^2}(\mathbf{x}, t; \mathbf{x}_s) - \nabla_{\mathbf{x}}^2 G(\mathbf{x}, t; \mathbf{x}_s) = \delta(\mathbf{x} - \mathbf{x}_s) \delta(t), \quad (1)$$

with  $G = 0, t < 0$ .

In common with all other migration methods, shot-geophone migration is based on the Born or single scattering approximation. Denote by  $r(\mathbf{x}) = \delta v(\mathbf{x})/v(\mathbf{x})$  a relative perturbation of the velocity field. Linearization of the wave equation yields for the corresponding perturbation of the Green's function

$$\frac{1}{v^2(\mathbf{x})} \frac{\partial^2 \delta G}{\partial t^2}(\mathbf{x}, t; \mathbf{x}_s) - \nabla_{\mathbf{x}}^2 \delta G(\mathbf{x}, t; \mathbf{x}_s) = \frac{2r(\mathbf{x})}{v^2(\mathbf{x})} \frac{\partial^2}{\partial t^2} G(\mathbf{x}, t; \mathbf{x}_s), \quad (2)$$

whose solution has the integral representation at the source and receiver points  $\mathbf{x}_r, \mathbf{x}_s$

$$\delta G(\mathbf{x}_r, t; \mathbf{x}_s) = \frac{\partial^2}{\partial t^2} \int d\mathbf{x} \frac{2r(\mathbf{x})}{v^2(\mathbf{x})} \int d\tau G(\mathbf{x}, t - \tau; \mathbf{x}_r) G(\mathbf{x}, \tau; \mathbf{x}_s). \quad (3)$$

The singly scattered field is the time convolution of  $\delta G$  with a source wavelet (or the space-time convolution with a radiation pattern operator, for more complex sources). Since the principal concern of this paper is kinematic relationships between data and image, we ignore the filtering by the source signature (i.e. replace it with a delta function). This effective replacement of the source by an impulse does not seem to invalidate the predictions of the theory, though the matter is certainly worthy of more study.

The Born modeling operator  $F[v]$  is

$$F[v]r(\mathbf{x}_r, t; \mathbf{x}_s) = \delta G(\mathbf{x}_r, t; \mathbf{x}_s). \quad (4)$$

## Common Offset Modeling and Migration

Basic versions of all prestack migration operators result from two further modeling steps:

- (i) extend the definition of reflectivity to depend on *more spatial degrees of freedom*, inserted somehow into the Born modeling formula (equation 2 or 3) in such a way that when the extra degrees of freedom are present in some specific way (“physical reflectivity”), Born modeling is recovered;
- (ii) form the adjoint of the extended modeling operator: this is a prestack migration operator. The output of the adjoint operator is the prestack image; it depends on the same degrees of freedom as the input of the modeling operator.

Prestack common offset modeling results from replacing  $2r(\mathbf{x})/v^2(\mathbf{x})$  with  $R(\mathbf{x}, \mathbf{h})$ , where  $\mathbf{h}$  is vector half-offset:  $\mathbf{h} = 0.5(\mathbf{x}_r - \mathbf{x}_s)$ .  $\mathbf{x}$  is not necessarily located below the midpoint. Denote by  $\mathbf{x}_m = 0.5(\mathbf{x}_r + \mathbf{x}_s)$  the corresponding midpoint vector.

The additional degrees of freedom mentioned in (i) above are the components of source-receiver half-offset. This extended reflectivity is inserted into the Born modeling formula to give the extended common offset modeling operator  $\bar{F}[v]$ :

$$\bar{F}_{\text{co}}[v]R(\mathbf{x}_r, t; \mathbf{x}_s) = u(\mathbf{x}_r, t; \mathbf{x}_s), \quad (5)$$

where

$$u(\mathbf{x}_m + \mathbf{h}, t; \mathbf{x}_m - \mathbf{h}) = \frac{\partial^2}{\partial t^2} \int d\mathbf{x} R(\mathbf{x}, \mathbf{h}) \int d\tau G(\mathbf{x}, t - \tau; \mathbf{x}_m + \mathbf{h}) G(\mathbf{x}, \tau; \mathbf{x}_m - \mathbf{h}). \quad (6)$$

If  $R(\mathbf{x}, \mathbf{h}) = 2r(\mathbf{x})/v^2(\mathbf{x})$  is actually independent of  $\mathbf{h}$ , then the output  $u(\mathbf{x}_r, t; \mathbf{x}_s)$  of equation 6 is identical to the perturbational Green’s function  $\delta G(\mathbf{x}_r, t; \mathbf{x}_s)$  as is clear from comparing equations 6 and 3. That is, the Born forward modeling operator is the “spray” operator ,

$$r(\mathbf{x}) \mapsto R(\mathbf{x}, \mathbf{h}) = 2r(\mathbf{x})/v^2(\mathbf{x}), \quad (7)$$

followed by the extended common offset modeling operator.

The common offset migration operator is the adjoint of this integral operator: its output is the offset-dependent prestack image volume, a function of the same type as the extended common offset reflectivity:

$$\begin{aligned} \bar{F}_{\text{co}}^*[v]d(\mathbf{x}, \mathbf{h}) &= I_{\text{co}}(\mathbf{x}, \mathbf{h}), \\ I_{\text{co}}(\mathbf{x}, \mathbf{h}) &= \int d\mathbf{x}_m \int dt \frac{\partial^2 d}{\partial t^2}(\mathbf{x}_m + \mathbf{h}, t; \mathbf{x}_m - \mathbf{h}) \int d\tau G(\mathbf{x}, t - \tau; \mathbf{x}_m + \mathbf{h}) G(\mathbf{x}, \tau; \mathbf{x}_m - \mathbf{h}). \end{aligned} \quad (8)$$

Therefore the adjoint of Born modeling (migration, *per se*) is common offset migration followed by the adjoint of the “spray” operator: this adjoint is the operator which sums or integrates in  $\mathbf{h}$ , that is, the *stack* operator.

Actually the operator defined in equation 8 is only one possible common offset migration operator. Many others follow through application of various weights, filters, and approximations. For example, leaving off the second time derivative in equation 8 amounts to filtering the data before application of  $\bar{F}_{\text{co}}^*[v]$ . Most notably, replacement of the Green’s functions in equation 8 by the leading terms in their high frequency asymptotic expansions results in the familiar Kirchhoff common offset migration operator. All of these variations define adjoints to (approximations of) the modeling operator with respect to appropriate inner products on domain and range spaces. Most important for this investigation, all share a common kinematic description. Therefore we ignore all such variations for the time being, and refer to equation 8 as defining “the” common offset migration operator.

Note that both modeling and migration operators share the property that their output for a given  $\mathbf{h}$  depends only on the input for the same value of  $\mathbf{h}$  - that is, they are *block-diagonal* on common offset data bins. This binwise action is responsible for the production of kinematic artifacts when the velocity field refracts rays sufficiently strongly (Stolk and Symes, 2004).

### Shot-geophone modeling and migration

Shot-geophone modeling results from a different extension of reflectivity: replace  $2r(\mathbf{x})/v^2(\mathbf{x})$  by  $R(\mathbf{x}, \mathbf{h})$  where  $\mathbf{h}$  is the depth (half)offset mentioned in the introduction. While this extension has exactly the same degrees of freedom as the common offset extended reflectivity, the two are conceptually quite different:  $\mathbf{h}$  here has *nothing to do* with the source-receiver half-offset  $0.5(\mathbf{x}_r - \mathbf{x}_s)$ !

The shot-geophone modeling operator  $\bar{F}[v]$  is given by

$$\bar{F}[v]R(\mathbf{x}_r, t; \mathbf{x}_s) = u(\mathbf{x}_r, t; \mathbf{x}_s), \quad (9)$$

where the field  $u$  is defined by

$$u(\mathbf{x}_r, t; \mathbf{x}_s) = \frac{\partial^2}{\partial t^2} \int d\mathbf{x} \int d\mathbf{h} R(\mathbf{x}, \mathbf{h}) \int d\tau G(\mathbf{x} + \mathbf{h}, t - \tau; \mathbf{x}_r) G(\mathbf{x} - \mathbf{h}, \tau; \mathbf{x}_s). \quad (10)$$

Note that here  $\mathbf{x}$  does play the role of midpoint, though having nothing to do with source-receiver midpoint.

The field  $u(\mathbf{x}, t; \mathbf{x}_s)$  is identical to  $\delta G(\mathbf{x}, t; \mathbf{x}_s)$  when

$$R(\mathbf{x}, \mathbf{h}) = \frac{2r(\mathbf{x})}{v^2(\mathbf{x})} \delta(\mathbf{h}), \quad (11)$$

i.e. when the generalized reflectivity is concentrated at offset zero. Therefore Born modeling is shot-geophone modeling following the mapping

$$r(\mathbf{x}) \mapsto \frac{2r(\mathbf{x})}{v^2(\mathbf{x})} \delta(\mathbf{h}). \quad (12)$$

The shot-geophone migration operator is the adjoint of the shot-geophone modeling operator: it produces an image volume with the same degrees of freedom as the extended shot-geophone reflectivity,

$$\begin{aligned} \bar{F}^*[v]d(\mathbf{x}, \mathbf{h}) &= I_{s-g}(\mathbf{x}, \mathbf{h}), \\ I_{s-g}(\mathbf{x}, \mathbf{h}) &= \int d\mathbf{x}_r \int d\mathbf{x}_s \int dt \frac{\partial^2 d}{\partial t^2}(\mathbf{x}_r, t; \mathbf{x}_s) \int d\tau G(\mathbf{x} + \mathbf{h}, t - \tau; \mathbf{x}_r) G(\mathbf{x} - \mathbf{h}, \tau; \mathbf{x}_s). \end{aligned} \quad (13)$$

Note that in both equations 10 and 13, all input variables are integrated to produce the value at each output vector: the computation is not block diagonal in  $\mathbf{h}$ , in contrast to the common offset operators defined in equations 6 and 8.

Born migration is shot-geophone migration followed by the adjoint of the mapping defined in equation 12, which is

$$R(\mathbf{x}, \mathbf{h}) \mapsto \frac{2R(\mathbf{x}, 0)}{v^2(\mathbf{x})}, \quad (14)$$

in other words, shot-geophone migration followed by extraction of the zero offset section.

For some purposes it turns out to be convenient to introduce *sunken source and receiver coordinates*

$$\bar{\mathbf{x}}_r = \mathbf{x} + \mathbf{h}, \quad \bar{\mathbf{x}}_s = \mathbf{x} - \mathbf{h}, \quad (15)$$

and the *source-receiver reflectivity*  $\bar{R}$  by

$$\bar{R}(\bar{\mathbf{x}}_r, \bar{\mathbf{x}}_s) = R\left(\frac{\bar{\mathbf{x}}_r + \bar{\mathbf{x}}_s}{2}, \frac{\bar{\mathbf{x}}_r - \bar{\mathbf{x}}_s}{2}\right), \text{ i.e. } \bar{R}(\mathbf{x} + \mathbf{h}, \mathbf{x} - \mathbf{h}) = R(\mathbf{x}, \mathbf{h}), \quad (16)$$

and similarly for the image volume  $I_{s-g}$ . Change integration variables in equation 13 to get the sunken source-receiver variant of shot-geophone migration:

$$\bar{I}_{s-g}(\bar{\mathbf{x}}_r, \bar{\mathbf{x}}_s) = \int d\mathbf{x}_r \int d\mathbf{x}_s \int dt \frac{\partial^2 d}{\partial t^2}(\mathbf{x}_r, t; \mathbf{x}_s) \int d\tau G(\bar{\mathbf{x}}_r, t - \tau; \mathbf{x}_r) G(\bar{\mathbf{x}}_s, \tau; \mathbf{x}_s). \quad (17)$$

Replacement of the Green's functions in this formula by their high-frequency asymptotic (ray-theoretic) approximations results in a Kirchhoff-like representation of shot-geophone migration.

## KINEMATICS OF SHOT-GEOPHONE MIGRATION

An event in the data is characterized by its moveout: locally, by a moveout equation  $t = T(\mathbf{x}_r, \mathbf{x}_s)$ , and infinitesimally by the source and receiver slownesses

$$\mathbf{p}_r = \nabla_{\mathbf{x}_r} T, \quad \mathbf{p}_s = \nabla_{\mathbf{x}_s} T \quad (18)$$

Significant energy with this moveout implies that locally near  $(\mathbf{x}_r, \mathbf{x}_s, t)$  the data contains a plane wave component with wavenumber  $(\omega \mathbf{p}_r, \omega \mathbf{p}_s, \omega)$ ,  $\omega$  being temporal frequency. These coordinates (position, wavenumber) give the phase space representation of the event.

Note that for incomplete coverage, notably marine streamer geometry, an event in the data will not determine its moveout uniquely. For example, in (idealized) marine streamer geometry, with the streamers oriented along the  $x$  axis, the  $y$  component of  $\mathbf{p}_r$  is not determined by the data. In the discussion to follow,  $\mathbf{p}_s$  and  $\mathbf{p}_r$  are assumed to be *compatible* with a reflection event.

Likewise, a reflector (in the source-receiver representation) at  $(\bar{\mathbf{x}}_r, \bar{\mathbf{x}}_s)$  with wavenumber  $(\mathbf{k}_r, \mathbf{k}_s)$  is characterized in (image volume) phase space by these coordinates.

### Kinematics with general (3D) offset

The kinematical description of shot-geophone migration relates the phase space coordinates of events and reflectors. An event with phase space representation

$$(\mathbf{x}_r, \mathbf{x}_s, T(\mathbf{x}_r, \mathbf{x}_s), \omega \mathbf{p}_r, \omega \mathbf{p}_s, \omega) \quad (19)$$

is the result of a reflector with (source-receiver) phase space representation  $(\bar{\mathbf{x}}_r, \bar{\mathbf{x}}_s, \mathbf{k}_r, \mathbf{k}_s)$  exactly when

- there is a ray  $(\mathbf{X}_s, \mathbf{P}_s)$  leaving the source point  $\mathbf{X}_s(0) = \mathbf{x}_s$  at time  $t = 0$  with ray parameter  $\mathbf{P}_s(0) = \mathbf{p}_s$ , and arriving at  $\mathbf{X}_s(t_s) = \bar{\mathbf{x}}_s$  at  $t = t_s$  with ray parameter  $\mathbf{P}_s(t_s) = -\mathbf{k}_s/\omega$ ;
- there is a ray  $(\mathbf{X}_r, \mathbf{P}_r)$  leaving  $\mathbf{X}_r(t_s) = \bar{\mathbf{x}}_r$  at  $t = t_s$  with ray parameter  $\mathbf{P}_r(t_s) = \mathbf{k}_r/\omega$  and arriving at the receiver point  $\mathbf{X}_r(t_r + t_s) = \mathbf{x}_s$  at time  $t = T(\mathbf{x}_r, \mathbf{x}_s) = t_r + t_s$  with ray parameter  $\mathbf{P}_r(t_r + t_s) = \mathbf{p}_r$ .

Figure 1 illustrates this kinematic relation. The Appendix provides a derivation.

Note that since  $\mathbf{P}_r, \mathbf{P}_s$  are ray slowness vectors, there is necessarily a length relation between  $\mathbf{k}_r, \mathbf{k}_s$ : namely,

$$\begin{aligned} \frac{1}{v(\bar{\mathbf{x}}_r)} &= \|\mathbf{P}_r(t_r)\| = \frac{\|\mathbf{k}_r\|}{|\omega|}, \\ \frac{1}{v(\bar{\mathbf{x}}_s)} &= \|\mathbf{P}_s(t_s)\| = \frac{\|\mathbf{k}_s\|}{|\omega|}, \end{aligned} \quad (20)$$

whence

$$\frac{\|\mathbf{k}_r\|}{\|\mathbf{k}_s\|} = \frac{v(\bar{\mathbf{x}}_s)}{v(\bar{\mathbf{x}}_r)} \quad (21)$$

The kinematics of shot-geophone migration are somewhat strange, so it is reassuring to see that for physical reflectors (i.e.  $R(\mathbf{x}, \mathbf{h}) = r(\mathbf{x})\delta(\mathbf{h})$ ) the relation just explained becomes the familiar one of reflection from a reflecting element according to Snell's law. A quick calculation shows that such a physical  $\bar{R}$  has a significant local plane wave component near  $(\bar{\mathbf{x}}_r, \bar{\mathbf{x}}_s)$  with wavenumber  $(\mathbf{k}_r, \mathbf{k}_s)$  only if  $\bar{\mathbf{x}}_r = \bar{\mathbf{x}}_s = \mathbf{x}$  and  $r$  has a significant local plane wave component near  $\mathbf{x}$  with wavenumber  $\mathbf{k}_x = \mathbf{k}_r + \mathbf{k}_s$ . From equation 21,  $\mathbf{k}_r$  and  $\mathbf{k}_s$  have the same length, therefore their sum  $\mathbf{k}_x$  is also their bisector, which establishes Snell's law. Thus a single (physical) reflector at  $\mathbf{x}$  with wavenumber  $\mathbf{k}_x$  gives rise to a reflected event at frequency  $\omega$  exactly when the rays  $(\mathbf{X}_s, \mathbf{P}_s)$  and  $(\mathbf{X}_r, \mathbf{P}_r)$  meet at  $\mathbf{x}$  at time  $t_s$ , and the reflector dip  $\mathbf{k}_x = \omega(\mathbf{P}_r(t_s) - \mathbf{P}_s(t_s))$ , which is the usual kinematics of single scattering. See Figure 2.

It is now possible to answer the question: in the shot-geophone model, to what extent does a data event determine the corresponding reflector? The rules derived above show

that the reflection point  $(\bar{\mathbf{x}}_s, \bar{\mathbf{x}}_r)$  must lie on the Cartesian product of two rays,  $(\mathbf{X}_s, \mathbf{P}_s)$  and  $(\mathbf{X}_r, \mathbf{P}_r)$ , consistent with the event, and the total time is also determined. If the coverage is complete, so that the event uniquely determines the source and receiver rays, then the source-receiver representation of the source-receiver reflector must lie along this uniquely determined ray pair. This fact contrasts dramatically with the imaging ambiguities prevalent in all forms of prestack depth migration based on data binning (Nolan and Symes, 1996; Nolan and Symes, 1997; Xu et al., 2001; Prucha et al., 1999; Brandsberg-Dahl et al., 2003; Stolk, 2002; Stolk and Symes, 2004). Even when coverage is complete, in these other forms of prestack migration strong refraction leads to multiple ray pairs connecting data events and reflectors, whence ambiguous imaging of a single event in more than one location within the prestack image volume.

Nonetheless reflector location is still not uniquely determined by shot-geophone migration as defined above, for two reasons:

- Only the total traveltimes is specified by the event! Thus if  $\bar{\mathbf{x}}_s = \mathbf{X}_s(t_s)$ ,  $\bar{\mathbf{x}}_r = \mathbf{X}_r(t_r)$  are related as described above to the event determining the ray pair, so is  $\bar{\mathbf{x}}'_s = \mathbf{X}_s(t'_s)$ ,  $\bar{\mathbf{x}}'_r = \mathbf{X}_r(t'_r)$  with  $t_s + t_r = t'_s + t'_r = t_{sr}$ . See Figure 1.
- Incomplete acquisition, for example limited to a narrow azimuth range as is commonly the case for streamer surveys, may prevent the event from determining its full 3D moveout, as mentioned above. Therefore a family of ray pairs, rather than a unique ray pair, may correspond to the event.

### Kinematics with horizontal offset

One way to view the remaining imaging ambiguity in shot-geophone migration as defined so far is to recognize that the image point coordinates  $(\bar{\mathbf{x}}_r, \bar{\mathbf{x}}_s)$  (or  $(\mathbf{x}, \mathbf{h})$ ) are six-dimensional (in 3D), whereas the data depend on only five coordinates  $(\mathbf{x}_r, t, \mathbf{x}_s)$  (at most). Formally, restricting one of the coordinates of the image point to be zero would at least make the variable counts equal, so that unambiguous imaging would at least be conceivable. Since physical reflectivities are concentrated at zero (vector) offset, it is natural to restrict one of the offset coordinates to be zero. The conventional choice, beginning with Claerbout's definition of survey-sinking migration (Claerbout, 1985), is the depth coordinate.

We assume that the shot-geophone reflectivity  $R(\mathbf{x}, \mathbf{h})$  takes the form

$$R(\mathbf{x}, \mathbf{h}) = R_z(\mathbf{x}, h_x, h_y)\delta(h_z), \quad (22)$$

leading to the restricted modeling operator:

$$\begin{aligned} \bar{F}_z[v]R_z(\mathbf{x}_r, t; \mathbf{x}_s) &= \frac{\partial^2}{\partial t^2} \int d\mathbf{x} \int dh_x \int dh_y \\ R_z(\mathbf{x}, h_x, h_y) &\int d\tau G(\mathbf{x} + (h_x, h_y, 0), t - \tau; \mathbf{x}_r)G(\mathbf{x} - (h_x, h_y, 0), \tau; \mathbf{x}_s). \end{aligned} \quad (23)$$

The kinematics of this restricted operator follows directly from that of the unrestricted operator, developed in the preceding section.

Denote  $\bar{\mathbf{x}}_s = (\bar{x}_s, \bar{y}_s, \bar{z}_s)$ ,  $\mathbf{k}_s = (k_{s,x}, k_{s,y}, k_{s,z})$  etc. For horizontal offset, the restricted form of the reflectivity in midpoint-offset coordinates (equation 22) implies a similarly restricted form for its description in sunken source-receiver coordinates:

$$\bar{R}(\bar{\mathbf{x}}_r, \bar{\mathbf{x}}_s) = \bar{R}_z \left( \bar{x}_r, \bar{x}_s, \bar{y}_r, \bar{y}_s, \frac{\bar{z}_r + \bar{z}_s}{2} \right) \delta(\bar{z}_r - \bar{z}_s). \quad (24)$$

Fourier transformation shows that  $\bar{R}$  has a significant plane wave component with wavenumber  $(\mathbf{k}_r, \mathbf{k}_s)$  precisely when  $\bar{R}_z$  has a significant plane wave component with wavenumber  $k_{r,x}, k_{r,y}, k_{s,x}, k_{s,y}, (k_{r,z} + k_{s,z})$ . Thus a ray pair  $(\mathbf{X}_r, \mathbf{P}_r), (\mathbf{X}_s, \mathbf{P}_s)$  compatible with a data event with phase space coordinates  $(\mathbf{x}_r, \mathbf{x}_s, T(\mathbf{x}_r, \mathbf{x}_s), \omega\mathbf{p}_r, \omega\mathbf{p}_s, \omega)$  images at a point  $X_{r,z}(t_s) = X_{s,z}(t_s) = z$ ,  $P_{r,z}(t_s) - P_{s,z}(t_s) = k_z/\omega$ ,  $X_{s,x}(t_s) = x_s$ ,  $P_{s,x}(t_s) = k_{s,x}/\omega$ , etc. at image phase space point

$$(\bar{x}_r, \bar{x}_s, \bar{y}_r, \bar{y}_s, z, k_{r,x}, k_{s,x}, k_{r,y}, k_{s,y}, k_z). \quad (25)$$

The adjoint of the modeling operator defined in equation 23 is the horizontal offset shot-geophone migration operator:

$$\bar{F}_z^*[v]d(\mathbf{x}, h_x, h_y) = I_{s-g,z}(\mathbf{x}, h_x, h_y), \quad (26)$$

where

$$\begin{aligned} I_{s-g,z}(\mathbf{x}, h_x, h_y) &= \int d\mathbf{x}_r \int d\mathbf{x}_s \int dt \\ \frac{\partial^2}{\partial t^2} d(\mathbf{x}_r, t; \mathbf{x}_s) &\int d\tau G(\mathbf{x} + (h_x, h_y, 0), t - \tau; \mathbf{x}_r)G(\mathbf{x} - (h_x, h_y, 0), \tau; \mathbf{x}_s). \end{aligned} \quad (27)$$

As mentioned before, operators and their adjoints enjoy the same kinematic relations, so we have already described the kinematics of this migration operator.

### Semblance property of horizontal offset image gathers and the DSR condition

As explained by Stolk and De Hoop (2001), Claerbout’s survey sinking migration is kinematically equivalent to shot-geophone migration as defined here, under two assumptions:

- subsurface offsets are restricted to horizontal ( $h_z = 0$ );
- rays (either source or receiver) carrying significant energy are nowhere horizontal, i.e.  $P_{s,z} > 0, P_{r,z} < 0$  throughout the propagation;
- events in the data determine full (four-dimensional) slowness  $\mathbf{P}_r, \mathbf{P}_s$ .

We call the second condition the “Double Square Root”, or “DSR”, condition, for reasons explained by Stolk and De Hoop (2001). This reference also offers a proof of the **Claim:** Under these restrictions, the imaging operator  $\bar{F}_z^*$  can image a ray pair at precisely one location in image volume phase space. When the velocity is correct, the image energy is therefore concentrated at zero offset in the image volume  $I_{s-g,z}$ .

The demonstration presented by Stolk and De Hoop (2001) uses oscillatory integral representations of the operator  $\bar{F}_z$  and its adjoint. However, the conclusion also follows directly from the kinematic analysis above and the DSR condition.

Indeed, note that the DSR condition implies that depth is increasing along the source ray, and decreasing along the receiver ray - otherwise put, depth is increasing along both rays, if you traverse the receiver ray *backwards*. Therefore depth can be used to parametrize the rays. With depth as the parameter, time is increasing from zero along the source ray, and decreasing from  $t_{sr}$  along the receiver ray (traversed backwards). Thus the two times can be equal (to  $t_s$ ) at exactly one point.

Since the scattering time  $t_s$  is uniquely determined, so are all the other phase space coordinates of the rays. If the ray pair is the incident-reflected ray pair of a reflector, then the reflector must be the *only* point at which the rays cross, since there is only one time  $t_s$  at which  $X_{s,z}(t_s) = X_{r,z}(t_s)$ . See Figure 3. Therefore in the infinite frequency limit the energy of this incident-reflected ray pair is imaged at zero offset, consistent with Claerbout’s imaging condition.

If furthermore coverage is complete, whence the data event uniquely determines the full slowness vectors, hence the rays, then it follows that a data event is imaged at precisely one location, namely the reflector which caused it, and in particular focusses at zero offset. This is the offset version of the result established by Stolk and De Hoop (2001), for which we have now given a different (and more elementary) proof.

**Remark:** Note that the DSR assumption precludes the imaging of near-vertical reflectors, since in general for such reflectors it will not be possible to satisfy the imaging conditions without either incident or reflected ray turning horizontal at some point.

### Semblance property of angle image gathers via Radon transform in offset and depth

According to Sava and Fomel (2003), angle image gathers  $A_z$  may be defined via Radon transform in offset and depth of the offset image gathers constructed above, i.e. the migrated data volume  $I_{s-g,z}(\mathbf{x}, h_x, h_y)$  (defined in equation 27) for fixed  $x, y$ :

$$A_z(x, y, \zeta, p_x, p_y) = \int dh_x \int dh_y I_{s-g,z}(x, y, \zeta + p_x h_x + p_y h_y, h_x, h_y), \quad (28)$$

in which  $\zeta$  denotes the  $z$ -intercept parameter, and  $p_x$  and  $p_y$  are the  $x$  and  $y$  components of offset ray parameter. The ray parameter components may then be converted to angle (Sava and Fomel, 2003). As is obvious from this formula, if the energy in  $I_{s-g,z}(\mathbf{x}, h_x, h_y)$  is focussed, i.e. localized, on  $h_x = 0, h_y = 0$ , then the Radon transform  $A_z$  will be (essentially) independent of  $p_x, p_y$ . That is, when displayed for fixed  $x, y$  with  $\zeta$  axis plotted vertically and  $p_x$  and  $p_y$  horizontally, the events in  $A_z$  will appear *flat*. The converse is also true. This is the semblance principle for angle gathers.

## SEMBLANCE PROPERTY OF ANGLE GATHERS VIA RADON TRANSFORM IN OFFSET AND TIME

The angle gathers defined by De Bruin et al. (1990) are based on migrated data  $D(\mathbf{x}, h_x, h_y, T)$ , i.e. depending on a time variable  $T$  in addition to the variables  $(\mathbf{x}, h_x, h_y)$ . Such migrated data is for example given by the following modification of equation 27

$$D(\mathbf{x}, h_x, h_y, T) = \int d\mathbf{x}_r \int d\mathbf{x}_s \int dt \frac{\partial^2}{\partial t^2} d(\mathbf{x}_r, t; \mathbf{x}_s) \int d\tau G(\mathbf{x} + (h_x, h_y, 0), t - T - \tau; \mathbf{x}_r) G(\mathbf{x} - (h_x, h_y, 0), \tau; \mathbf{x}_s). \quad (29)$$

As we have done with other fields, we denote by  $\bar{D}$  the field  $D$  referred to sunken source and receiver coordinates.

Again this migration formula can be obtained as the adjoint of a modified forward map, mapping an extended reflectivity to data, similarly as above. In this case the extended reflectivity depends on the variables  $(\mathbf{x}, h_x, h_y, T)$ , with physical reflectivity given by  $r(\mathbf{x})\delta(h_x)\delta(h_y)\delta(T)$ . This physical reflectivity is obtained by a time injection operator

$$(J_t \bar{R}_z)(\bar{x}_r, \bar{x}_s, \bar{y}_r, \bar{y}_s, \bar{z}, t) = \bar{R}_z(\bar{x}_r, \bar{x}_s, \bar{y}_r, \bar{y}_s, \bar{z})\delta(t). \quad (30)$$

To obtain a migrated image volume, the extraction of zero offset data in equation 14. is preceded by extracting the  $T = 0$  data from  $D$ . It is indeed clear that setting  $T$  to zero in equation 29 yields the shot-geophone migration output defined in equation 27.

Angle gathers obtained via Radon transform in offset and time of  $D(\mathbf{x}, h_x, h_y, T)$  were introduced by (de Bruin et al., 1990), and discussed further in (Prucha et al., 1999). We denote these gathers by

$$B_z(\mathbf{x}, p_x, p_y) = \int dh_x \int dh_y D(\mathbf{x}, h_x, h_y, p_x h_x + p_y h_y). \quad (31)$$

The purpose of this section is to establish the semblance property of the angle gathers  $B_z$ .

Note that the Radon transform in equation 31 is evaluated at zero (time) intercept. The dependence on  $z$  is carried by the coordinate plane in which the Radon transform is performed, rather than by the  $(z-)$  intercept as was the case with the angle gathers  $A_z$  defined previously. Also note that  $B_z$  requires the double square root field  $D$ , whereas  $A_z$  may be constructed with the image output by any version of shot-geophone migration.

We first need to establish at which points  $(\mathbf{x}, h_x, h_y, T)$  significant energy of  $D(\mathbf{x}, h_x, h_y, T)$  is located. The argument for  $\bar{D}$  is slightly different from the argument for  $\bar{I}_z$ , since  $\bar{D}$  depends also on the time. For  $\bar{I}_z$  there was a kinematic relation  $(\mathbf{x}_s, \mathbf{x}_r, t_{sr}, \omega \mathbf{p}_s, \omega \mathbf{p}_r, \omega)$  to a point in phase space  $(x_s, x_r, y_s, y_r, z, k_{s,x}, k_{r,x}, k_{s,y}, k_{r,y}, k_z)$  where the energy in  $\bar{I}_z$  is located. The restriction of  $\bar{D}$  to time  $T$  is the same as the restriction to time 0, but using time-shifted data  $d(\dots, t + T)$ . Therefore we can follow almost the same argument as for the kinematic relation of  $\bar{I}_z$ . We find that for an event at  $(\mathbf{x}_s, \mathbf{x}_r, t_{sr}, \omega \mathbf{p}_s, \omega \mathbf{p}_r, \omega)$  to contribute at  $\bar{D}$ , restricted to time  $T$ , we must have that  $(x_s, y_s, z)$  is on the ray  $\mathbf{X}_s$ ,

say at time  $t'_s$ , i.e.  $(x_s, y_s, z) = \mathbf{X}_s(t'_s)$ . Then  $(x_r, y_r, z)$  must be on the ray  $\mathbf{X}_r$  say at time  $t''_s$ , i.e.  $(x_r, y_r, z) = \mathbf{X}_r(t''_s)$ . The situation is displayed in Figure 4, using midpoint-offset coordinates. Furthermore, the sum of the traveltimes from  $\mathbf{x}_s$  to  $(x_s, y_s, z)$  and from  $\mathbf{x}_r$  to  $(x_r, y_r, z)$  must be equal to  $t_{sr} - T$ . It follows that  $t''_s - t'_s = T$ .

Now consider an event from a physical reflection at  $\mathbf{X}_s(t_s) = \mathbf{X}_r(t_s) = (x_{\text{scat}}, y_{\text{scat}}, z_{\text{scat}})$ . We use the previous reasoning to find where the energy in  $D$  is located (in midpoint-offset coordinates). We will denote by  $(v_{s,x}(t), v_{s,y}(t), v_{s,z}(t))$  the ray velocity for the source ray  $\frac{d\mathbf{X}_s}{dt}$ . The horizontal “sunken source” coordinates  $(x - h_x, y - h_y)$  then satisfy

$$x_{\text{scat}} - (x - h_x) = \int_{t'_s}^{t_s} dt v_{s,x}(t), \quad y_{\text{scat}} - (y - h_y) = \int_{t'_s}^{t_s} dt v_{s,y}(t), \quad (32)$$

For the “sunken receiver” coordinates we find

$$(x + h_x) - x_{\text{scat}} = \int_{t_s}^{t''_s} dt v_{r,x}(t), \quad (y + h_y) - y_{\text{scat}} = \int_{t_s}^{t''_s} dt v_{r,y}(t). \quad (33)$$

Adding up the  $x$  components of these equations, and separately the  $y$  components of these equations gives that

$$2h_x = \int_{t'_s}^{t''_s} v_x(t) dt, \quad 2h_y = \int_{t'_s}^{t''_s} v_y(t) dt, \quad (34)$$

where now the velocity  $(v_x(t), v_y(t))$  is from the source ray for  $t < t_s$ , and from the receiver ray for  $t > t_s$ . Let us denote by  $v_{\parallel, \max}$  the maximal horizontal velocity along the rays between  $(x_{\text{scat}}, y_{\text{scat}}, z_{\text{scat}})$  and the points  $(x_s, y_s, z)$  and  $(x_r, y_r, z)$ , then we have

$$2\|(h_x, h_y)\| \leq |t''_s - t'_s| v_{\parallel, \max} = |T| v_{\parallel, \max}. \quad (35)$$

For the 2D case we display the situation in Figure 5. The energy in  $\bar{D}$  is located in the shaded region of the  $(h_x, T)$  plane indicated in the Figure. In 3D this region becomes a cone.

The angle transform in equation 31 is an integral of  $D$  over a plane in the  $(h_x, h_y, T)$  volume given by

$$T = p_x h_x + p_y h_y. \quad (36)$$

Suppose now that

$$\sqrt{p_x^2 + p_y^2} < \frac{2}{v_{\parallel, \max}}, \quad (37)$$

Then we have

$$|T| = |p_x h_x + p_y h_y| < \frac{2}{v_{\parallel, \max}} \sqrt{h_x^2 + h_y^2}. \quad (38)$$

In the 2D Figure 5 this means that the lines of integration are not in the shaded region of the  $(h_x, T)$  plane. In 3D, the planes of integration are not in the corresponding cone. The only points where the planes of integration intersect the set of  $(h_x, h_y, T)$  where energy of  $D$  is located, are points with  $T = 0, h_x = h_y = 0$ . It follows that the energy in the angle transform of equation 31 is located only at the true scattering point independent of  $(p_x, p_y)$ . We conclude that the semblance property also holds for the angle transform via Radon transform in the offset time domain, provided that 37 holds.

The bound  $v_{\parallel, \max}$  need not be a global bound on the horizontal component of the ray velocity. The integral in equation 31 is over some finite range of offsets, hence on some finite range of times, so that the distance between say the midpoint  $\mathbf{x}$  in equation 31, and the physical scattering point is bounded. Therefore  $v_{\parallel, \max}$  should be a bound on the horizontal component of the ray velocity on some sufficiently large region around  $\mathbf{x}$ .

## EXAMPLES

In three 2D synthetic data examples we illustrate the semblance property established in the preceding pages for shot-geophone migration. These examples expose the dramatic contrast between image (or common-image-point) gathers produced by shot-geophone migration and those produced by other forms of prestack depth migration. In all three examples, the formation of caustics leads to failure of the semblance principle for Kirchhoff (or Generalized Radon Transform) common scattering angle migration (Xu et al., 2001; Brandsberg-Dahl et al., 2003). In all three examples the DSR assumption is satisfied for the acquisition offsets considered. For the shot-geophone migration we employ the double square root approach, using a generalized screen propagator (GSP) approximation of the square root operator (Le Rousseau and De Hoop, 2001). We form angle image gathers by Radon transform in offset and time, following (de Bruin et al., 1990; Prucha et al., 1999). Conversion of ‘slope’ to scattering angle follows the method described by De Hoop et al. (2003, equations 88-89).

## Lens model

This example is used in (Stolk, 2002; Stolk and Symes, 2004) to show that common offset and Kirchhoff (or generalized Radon transform) common scattering-angle migration produce strong kinematic artifacts in strongly refracting velocity models. The velocity model lens embedded in a constant background. This model is strongly refracting through the formation of triplications in the rayfields. Below the lens, at a depth of 2 km, we placed a flat, horizontal reflector. We synthesized data using a (4, 10, 20, 40) Hz zero phase bandpass filter as (isotropic) source wavelet, and a finite difference scheme with adequate sampling. A typical shot gather over the lens (Figure 8, shot position indicated by a vertical arrow in Figure 6) shows a complex pattern of reflections from the flat reflector that have propagated through the lens.

We migrated the data with the above mentioned depth-extrapolation approach. Figure 7 shows the image, which clearly reproduces the reflector. An angle image gather is shown in Figure 10; for comparison we show the Kirchhoff common scattering angle image gather in Figure 9) at the same location (left) reproduced from (Stolk and Symes, 2004), each trace of which is obtained by Kirchhoff migration restricted to common angle. The Kirchhoff image gather is clearly contaminated by numerous energetic non-flat events, while the wave equation image gather is not. Artifacts in the Kirchhoff image gather must be non flat and can be removed by ‘dip’ filtering in depth and angle, but only if the velocity model is perfectly well known. In the wave equation image gather we observe a hint of residual moveout, which we attribute to reduced accuracy of the DSR propagator at large propagation angles. The image gathers have an increase in amplitude with increase in scattering angle in common.

## Valhall lens model

This example is used in (Brandsberg-Dahl et al., 2003). The compressional-wave velocity model (Figure 11) is a simplification of the geological setting of the Valhall field. The model is in fact isotropic elastic, but the main heterogeneity appears in the compressional wave velocity. It consists of a slow Gaussian lens (gas); below the lens, at a depth of 1.5 km, we placed a reflector that is partly horizontal (a reservoir) and partly dipping to the left. One can view the dipping part of the reflector as a model fault plane. Above the

reflector, the Gaussian lens is embedded in a constant gradient ( $0.45 \text{ s}^{-1}$ ) background; below the reflector the velocity is constant. Again, this model is strongly refracting.

We synthesized multi-component elastic-wave data using a bandpass filter with dominant frequency 35 Hz as (isotropic, explosive) source wavelet, and a finite difference scheme with close to adequate sampling. (Some numerical dispersion is present, but the sampling would have been unrealistically fine to remove all dispersive effects associated with relatively low shear-wave velocities.) We extract the vertical component to suppress the shear-wave contributions. A typical shot gather over the lens (Figure 13, vertical component, shot position indicated by a vertical arrow in Figure 11) shows a complex pattern of reflections from the reflector propagated through the lens; we note the weak, remaining contributions from mode converted waves at later times that will not be treated properly by our acoustic-wave migration scheme here.

We migrated the data with the above mentioned depth-extrapolation approach. Figure 12 shows the image. An angle image gather (at horizontal location indicated by a vertical line in Figure 11) is shown in Figure 14 (right); for comparison we show the angle image gather at the same location (left) reproduced from (Brandsberg-Dahl et al., 2003), which is obtained by generalized Radon transform migration (without focussing in dip or the application of isochron filters). The left image gather is, again, clearly contaminated by energetic non-flat events, while the right image gather is not.

### **Marmousi derived model**

To establish the absence of artifacts in a geologically yet more realistic model, we adopt a model derived from the Marmousi model (Xu et al., 2001). It is based on a smoothing of the Marmousi velocity model and superimposing a layer of thickness 100 m and contrast 10 m/s at depth 2400 m (Figure 15 (top)). The smoothing was carried out with a low-pass filter, Gaussian shaped of half-power radius 150 m.

The data were generated, using an appropriately sampled finite difference scheme, as the difference between the data in the smooth, reference, model (without the layer) and the data in the model with the layer. The source was isotropic and dilational; the source wavelet was obtained as a (5, 13, 40, 55) Hz bandpass filter – with a time delay of 56 ms. Multi-pathing is prevalent in the right part of the model. A typical shot gather is shown

in Figure 16 with shot position indicated by a vertical arrow in Figure 15 (top)); it shows, again, a very complex pattern of reflections.

We migrated the data with the above mentioned depth-extrapolation approach. Figure 15 (right) shows the image, in which the two reflectors are clearly resolved. An angle image gather (at horizontal location indicated by a vertical line in Figure 15 (top)) is shown in Figure 17 (right); for comparison we show the angle image gather at the same location (left) reproduced from (Stolk and Symes, 2004), each trace of which is obtained by Kirchhoff migration restricted to common scattering angle. The left image gather is, again, contaminated by energetic non-flat events; one artifact is indicated by a curve. The right image gather does not contain artifacts, as expected.

## CONCLUSION

We have demonstrated, mathematically and by example, that shot-geophone migration produces artifact-free image volumes, assuming (i) kinematically correct and relatively smooth velocity model, (ii) incident energy traveling downwards, reflected energy traveling upwards, and (iii) enough data to uniquely determine rays corresponding to events in the data. The examples compared shot-geophone migration with Kirchhoff common scattering angle migration. While the latter technique bins data only implicitly, it is like other binwise migration schemes, such as common offset migration, in generating kinematic image artifacts in prestack data when the velocity model is sufficiently complex to strongly refract waves.

The recent literature contains a number of comparisons of Kirchhoff and wave equation migration (for example, (Albertin et al., 2002; Fliedner et al., 2002)). Performance differences identified in these reports have been ascribed to a wide variety of factors, such as differences in anti-aliasing and decimation strategies, choice of time fields used in Kirchhoff imaging, and “fidelity” to the wave equation. These factors surely affect performance, but reflect mainly implementation decisions. The difference identified and demonstrated in this paper, on the other hand, is *fundamental*: it flows from the differing formulations of prestack imaging (and modeling) underlying the two classes of methods. No implementation variations can mask it.

In fact, we have shown that implementation has at most a secondary impact on kinematic accuracy of shot-geophone imaging. Its basic kinematics is shared not just by the two common depth extrapolation implementations - shot profile, double square root - but also by a variant of reverse time imaging and even by a Kirchhoff or Generalized Radon Transform operator of appropriate construction. Naturally these various options differ in numerous ways, in their demands on data quality and sampling and in their sensitivity to various types of numerical artifacts. However in the ideal limit of continuous data and discretization-free computation, all share an underlying kinematic structure and offer the potential of artifact-free data volumes when the assumptions of our theory are satisfied, even in the presence of strong refraction and multiple arrivals at reflecting horizons.

It remains to address three shortcomings of the theory. The first is its reliance on the “DSR” assumption, i.e. no turning rays. The numerical investigations of Biondi and Shan (2002) suggested that reverse time (two-way) wave equation migration, as presented here, could be modified by inclusion of nonhorizontal offsets to permit the use of turning energy, and indeed to image reflectors of arbitrary dip. This latter possibility has been understood in the context of (stacked) images for some time (Yoon et al., 2003). Biondi and Shan (2002) present prestack image gathers for horizontal and vertical offsets which suggest that a similar flexibility may be available for the shot-geophone extension. Biondi and Symes (2004) give a local analysis of shot-geophone image formation using nonhorizontal offsets, whereas Symes (2002) studied globally the formation of kinematic artifacts in a horizontal / vertical offset image volume. In contrast to the horizontal offset / DSR setting, such artifacts in general offset shot-geophone image volumes cannot be entirely ruled out. However kinematic artifacts cannot occur at arbitrarily small offset, in contrast to the formation of artifacts at all offsets in binwise migration.

A second limitation of our main result is its assumption that ray kinematics are completely determined by the data. Of course this is no limitation for the 2D synthetic examples presented above. “True 3D” acquisition is not unknown (Brandsberg-Dahl et al., 2003), but is uncommon - most contemporary data is acquired with narrow-azimuth streamer equipment. For such data, we cannot in general rule out the appearance of artifacts due to multiple ray pairs satisfying the shot-geophone kinematic imaging conditions. However two observations suggest that all is not lost. First, for ideal “2.5D” structure

(independent of crossline coordinate) and perfect linear survey geometry (no feathering), all energetic rays remain in the vertical planes through the sail line, and our analysis applies without alteration to guarantee imaging fidelity. Second, the conditions that ensure absence of artifacts are *open*, i.e. small perturbations of velocity and source and receiver locations cannot affect the conclusion. Therefore shot-geophone imaging fidelity is robust against mild crossline heterogeneity and small amounts of cable feathering. Note that nothing about the *formulation* of our modeling or (adjoint) migration operators requires areal geometry - the operators are perfectly well-defined for narrow azimuth data.

A very intriguing and so far theoretically untouched area concerns the potential of *multiple* narrow azimuth surveys, with distinct central azimuths, to resolve the remaining ambiguities of single azimuth imaging.

A third, and much more fundamental, limitation pertains to migration itself. Migration operators are essentially adjoints to *linearized* modeling operators. The kinematic theory of migration requires that the velocity model be slowly varying on the wavelength scale, or at best be slowly varying except for a discrete set of fixed, regular interfaces. The most challenging contemporary imaging problems, for example subsalt prospect assessment, transgress this limitation, in many cases violently. Salt-sediment interfaces are amongst the unknowns, especially bottom salt, are quite irregular, and are perhaps not even truly interfaces. Very clever solutions have been and are being devised for these difficult imaging problems, but the theory lags far, far behind the practice.

### Acknowledgements

This work was supported in part by National Science Foundation, and by the sponsors of The Rice Inversion Project (TRIP). MdH also acknowledges support by Total E&P USA. We thank A. E. Malcolm for her help in generating the examples, Gilles Lambaré for provision of the Marmousi-derived data, and Norman Bleistein for careful scrutiny of an early draft.

### References

Albertin, U., Watts, D., Chang, W., Kapoor, S. J., Stork, C., Kitchenside, P., and Yingst, D., 2002, Near-salt-flank imaging with kirchhoff and wavefield-extrapolation migration:

- 72nd Annual International Meeting, Society of Exploration Geophysicists, Expanded Abstracts, 1328–1331.
- Biondi, B., and Shan, G., 2002, Prestack imaging of overturned reflections by reverse time migration: 72nd Annual International Meeting, Society of Exploration Geophysicists, Expanded Abstracts, 1284–1287.
- Biondi, B., and Symes, W., 2004, Angle-domain common-image gathers for migration velocity analysis by wavefield-continuation imaging: *Geophysics*, **69**, 1283–1298.
- Brandsberg-Dahl, S., De Hoop, M., and Ursin, B., 2003, Focusing in dip and AVA compensation on scattering angle/azimuth common image gathers: *Geophysics*, **68**, 232–254.
- Claerbout, J. F., 1971, Toward a unified theory of reflector mapping: *Geophysics*, **36**, 467–481.
- Claerbout, J., 1985, *Imaging the earth's interior*: Blackwell Scientific Publishers, Oxford.
- de Bruin, C. G. M., Wapenaar, C. P. A., and Berkhout, A. J., 1990, Angle-dependent reflectivity by means of prestack migration: *Geophysics*, **55**, 1223–1234.
- De Hoop, M., Le Rousseau, J., and Biondi, B., 2003, Symplectic structure of wave-equation imaging: A path-integral approach based on the double-square-root equation: *Geoph. J. Int.*, **153**, 52–74.
- Duistermaat, J., *Fourier integral operators*:, Lecture notes, Courant Institute, New York, 1973.
- Fliedner, M. M., Crawley, S., Bevc, D., Popovici, A. M., and Biondi, B., 2002, Imaging of a rugose salt body in the deep gulf of Mexico: Kirchhoff versus common azimuth wave-equation migration: 72nd Annual International Meeting, Society of Exploration Geophysicists, Expanded Abstracts, 1304–1307.
- Hormander, L., 1983, *The analysis of linear partial differential operators*:, volume I Springer Verlag, Berlin.

- Kleyn, A., 1983, Seismic reflection interpretation: Applied Science Publishers, New York.
- Le Rousseau, J., and De Hoop, M., 2001, Modeling and imaging with the scalar generalized-screen algorithms in isotropic media: *Geophysics*, **66**, 1551–1568.
- Nolan, C. J., and Symes, W. W., 1996, Imaging and conherency in complex structure: 66th Annual International Meeting, Society of Exploration Geophysicists, Expanded Abstracts, 359–363.
- Nolan, C., and Symes, W., 1997, Global solution of a linearized inverse problem for the wave equation: *Comm. P. D. E.*, **22**, 919–952.
- Prucha, M., Biondi, B., and Symes, W., 1999, Angle-domain common image gathers by wave-equation migration: 69th Annual International Meeting, Society of Exploration Geophysicists, Expanded Abstracts, 824–827.
- Rakesh, 1988, A linearized inverse problem for the wave equation: *Comm. on P.D.E.*, **13**, no. 5, 573–601.
- Sava, P., and Fomel, S., 2003, Angle-domain common-image gathers by wavefield continuation methods: *Geophysics*, **68**, 1065–1074.
- Schultz, P., and Sherwood, J., 1982, Depth migration before stack: *Geophysics*, **45**, 376–393.
- Shen, P., Symes, W., and Stolk, C., 2003, Differential semblance velocity analysis by wave-equation migration: 73rd Annual International Meeting, Society of Exploration Geophysicists, Expanded Abstracts, 2135–2139.
- Stolk, C. C., and De Hoop, M. V., December 2001, Seismic inverse scattering in the ‘wave-equation’ approach, Preprint 2001-047, The Mathematical Sciences Research Institute, <http://msri.org/publications/preprints/2001.html>.
- Stolk, C. C., and Symes, W. W., 2004, Kinematic artifacts in prestack depth migration: *Geophysics*, **69**, 562–575.
- Stolk, C. C., 2002, Microlocal analysis of the scattering angle transform: *Comm. P. D. E.*, **27**, 1879–1900.

Symes, W. W., 2002, Kinematics of Reverse Time Shot-Geophone Migration, The Rice Inversion Project, Department of Computational and Applied Mathematics, Rice University, Houston, Texas, USA: <http://www.trip.caam.rice.edu>.

Taylor, M., 1981, Pseudodifferential operators: Princeton University Press, Princeton, New Jersey.

Xu, S., Chauris, H., Lambaré, G., and Noble, M., 2001, Common angle migration: A strategy for imaging complex media: *Geophysics*, **66**, no. 6, 1877–1894.

Yilmaz, O., 1987, Seismic data processing: Investigations in Geophysics No. 2.

Yoon, K., Shin, C., Suh, S., Lines, L., and Hong, S., 2003, 3d reverse-time migration using the acoustic wave equation: An experience with the SEG/EAGE data set: *The Leading Edge*, **22**, 38.

## APPENDIX

In this appendix we establish the relation between the appearance of events in the data and the presence of reflectors in the migrated image. This relation is the *same* for the forward modeling operator and for its adjoint, the migration operator.

The reasoning presented here shares with (Stolk and De Hoop, 2001) the identification of events, respectively reflectors, by high frequency asymptotics in phase space, but differs in that it does not explicitly use oscillatory integral representations of  $F[v]$ . Instead, this argument follows the pattern of Rakesh’s analysis of shot profile migration kinematics (Rakesh, 1988). It can be made mathematically rigorous, by means of the so-called Gabor calculus in the harmonic analysis of singularities (see (Duistermaat, 1973) Ch. 1).

Our analysis is based on the recognition that the shot-geophone predicted data field  $u(\mathbf{x}_r, t; \mathbf{x}_s)$ , defined by equation 10, is the value at  $\bar{\mathbf{x}} = \mathbf{x}_r$  of the space-time field  $u(\bar{\mathbf{x}}, t; \mathbf{x}_s)$ , which solves

$$\frac{1}{v^2(\bar{\mathbf{x}})} \frac{\partial^2 u}{\partial t^2}(\bar{\mathbf{x}}, t; \mathbf{x}_s) - \nabla_{\bar{\mathbf{x}}}^2 u(\bar{\mathbf{x}}, t; \mathbf{x}_s) = \int d\mathbf{h} R(\bar{\mathbf{x}} - \mathbf{h}, \mathbf{h}) \frac{\partial^2}{\partial t^2} G(\bar{\mathbf{x}} - 2\mathbf{h}, t; \mathbf{x}_s) \quad (\text{A-1})$$

This equation follows directly by applying the wave operator to both sides of equation 10.

The appearance of an event at a point  $(\mathbf{x}_s, \mathbf{x}_r, t_{sr})$  in the data volume is equivalent to the presence of a sizeable Fourier coefficient for a plane wave component

$$e^{i\omega(t - \mathbf{p}_s \cdot \bar{\mathbf{x}}_s - \mathbf{p}_r \cdot \bar{\mathbf{x}}_r)} \quad (\text{A-2})$$

in the acoustic field for frequencies  $\omega$  within the bandwidth of the data, even after muting out all events at a small distance from  $(\mathbf{x}_s, \mathbf{x}_r, t_{sr})$ .

Note that the data does not necessarily fully determine this plane wave component, i.e. the full 3D event slownesses  $\mathbf{p}_s, \mathbf{p}_r$ . In this appendix,  $\mathbf{p}_s, \mathbf{p}_r$  are assumed to be compatible with the data, in the sense just explained.

Assume that these frequencies are high enough relative to the length scales in the velocity that such local plane wave components propagate according to geometric acoustics. This assumption tacitly underlies much of reflection processing, and in particular is vital to the success of migration.

That is, solutions of wave equations such as A-1 carry energy in local plane wave components along rays. Let  $(\mathbf{X}_r(t), \mathbf{P}_r(t))$  denote such a ray, so that  $\mathbf{X}_r(t_{sr}) = \mathbf{x}_r, \mathbf{P}_r(t_{sr}) = \mathbf{p}_r$ . Then at some point the ray must pass through a point in phase space at which the source term (right hand side) of equation A-1 has significant energy - otherwise the ray would never pick up any energy at all, and there would be no event at time  $t_{sr}$ , receiver position  $\mathbf{x}_r$ , and receiver slowness  $\mathbf{p}_r$ . [Supplemented with proper mathematical boilerplate, this statement is the celebrated *Propagation of Singularities* theorem of Hörmander, (Hörmander, 1983; Taylor, 1981).]

The source term involves (i) a product, and (ii) an integral in some of the variables. The Green's function  $G(\bar{\mathbf{x}}_s, t, \mathbf{x}_s)$  has high frequency components along rays from the source, i.e. at points of the form  $(\mathbf{X}_s(t_s), \mathbf{P}_s(t_s))$  where  $\mathbf{X}_s(0) = \mathbf{x}_s$  and  $t_s \geq 0$ . [Of course this is just another instance of Propagation of Singularities, as the source term in the wave equation for  $G(\bar{\mathbf{x}}_s, t_s, \mathbf{x}_s)$  is singular only at  $(\mathbf{x}_s, 0)$ .] That is, viewed as a function of  $\bar{\mathbf{x}}_s$  and  $t_s$ ,  $G(\cdot, \cdot; \mathbf{x}_s)$  will have significant Fourier coefficients for plane waves

$$e^{i\omega(\mathbf{P}_s(t_s) \cdot \bar{\mathbf{x}}_s + t_s)} \quad (\text{A-3})$$

We characterize *reflectors* in the same way: that is, there is a (double) reflector at  $(\bar{\mathbf{x}}_s, \bar{\mathbf{x}}_r)$  if  $\bar{R}$  has significant Fourier coefficients of a plane wave

$$e^{i(\mathbf{k}_s \cdot \bar{\mathbf{x}}'_s + \mathbf{k}_r \cdot \bar{\mathbf{x}}'_r)} \quad (\text{A-4})$$

for some pair of wavenumbers  $\mathbf{k}_s, \mathbf{k}_r$ , and for generic points  $(\bar{\mathbf{x}}'_s, \bar{\mathbf{x}}'_r)$  near  $(\bar{\mathbf{x}}_s, \bar{\mathbf{x}}_r)$ . Presumably then the product  $R(\bar{\mathbf{x}}'_s, \mathbf{x})G(\bar{\mathbf{x}}'_s, t_s; \mathbf{x}_s)$  has a significant coefficient of the plane wave component

$$e^{i((\mathbf{k}_s + \omega \mathbf{P}_s(t_s)) \cdot \bar{\mathbf{x}}'_s + \mathbf{k}_r \cdot \mathbf{x} + \omega t_s)} \quad (\text{A-5})$$

for  $\bar{\mathbf{x}}'_s$  near  $\bar{\mathbf{x}}_s$ ,  $\mathbf{x}$  near  $\bar{\mathbf{x}}_r$ ; note that implicitly we have assumed that  $\bar{\mathbf{x}}_s$  (the argument of  $G$ ) is located on a ray from the source with time  $t_s$ . The right-hand side of equation A-1 integrates this product over  $\bar{\mathbf{x}}_s$ . This integral will be negligible unless the phase in  $\bar{\mathbf{x}}_s$  is stationary: that is, to produce a substantial contribution to the RHS of equation A-1, it is necessary that

$$\bar{\mathbf{x}}_s = \mathbf{X}_s(t_s), \quad \mathbf{k}_s + \omega \mathbf{P}_s(t_s) = 0 \quad (\text{A-6})$$

Supposing that this is so, the remaining exponential suggests that the RHS of equation A-1 has a sizeable passband component of the form

$$e^{i(\mathbf{k}_r \cdot \mathbf{x} + \omega t_s)} \quad (\text{A-7})$$

for  $\mathbf{x}$  near  $\bar{\mathbf{x}}_r$ . As was argued above, this RHS will give rise to a significant plane wave component in the solution  $u$  arriving at  $\mathbf{x}_r$  at time  $t_{sr} = t_s + t_r$  exactly when a ray arriving at  $\mathbf{x}_r$  at time  $t_{sr}$  starts from a position in space-time with the location and wavenumber of this plane wave, at time  $t_s = t_{sr} - t_r$ : that is,

$$\mathbf{X}_r(t_s) = \bar{\mathbf{x}}_r, \quad \omega \mathbf{P}_r(t_s) = \mathbf{k}_r \quad (\text{A-8})$$

We end this appendix with a remark about the case of *complete coverage*, i.e. sources and receivers densely sample a fully 2D area on or near the surface. Assuming that the effect of the free surface has been removed, so that all events may be viewed as samplings of an upcoming wavefield, the data (2D) event slowness uniquely determines the wavefield (3D) slowness through the eikonal equation. Thus an event in the data is characterized by its (3D) moveout: locally, by a moveout equation  $t = T(\mathbf{x}_s, \mathbf{x}_r)$ , and infinitesimally by the source and receiver slownesses

$$\mathbf{p}_s = \nabla_{\mathbf{x}_s} T, \quad \mathbf{p}_r = \nabla_{\mathbf{x}_r} T \quad (\text{A-9})$$

In this case, the data event uniquely determines the source and receiver rays.

Figure number: 1

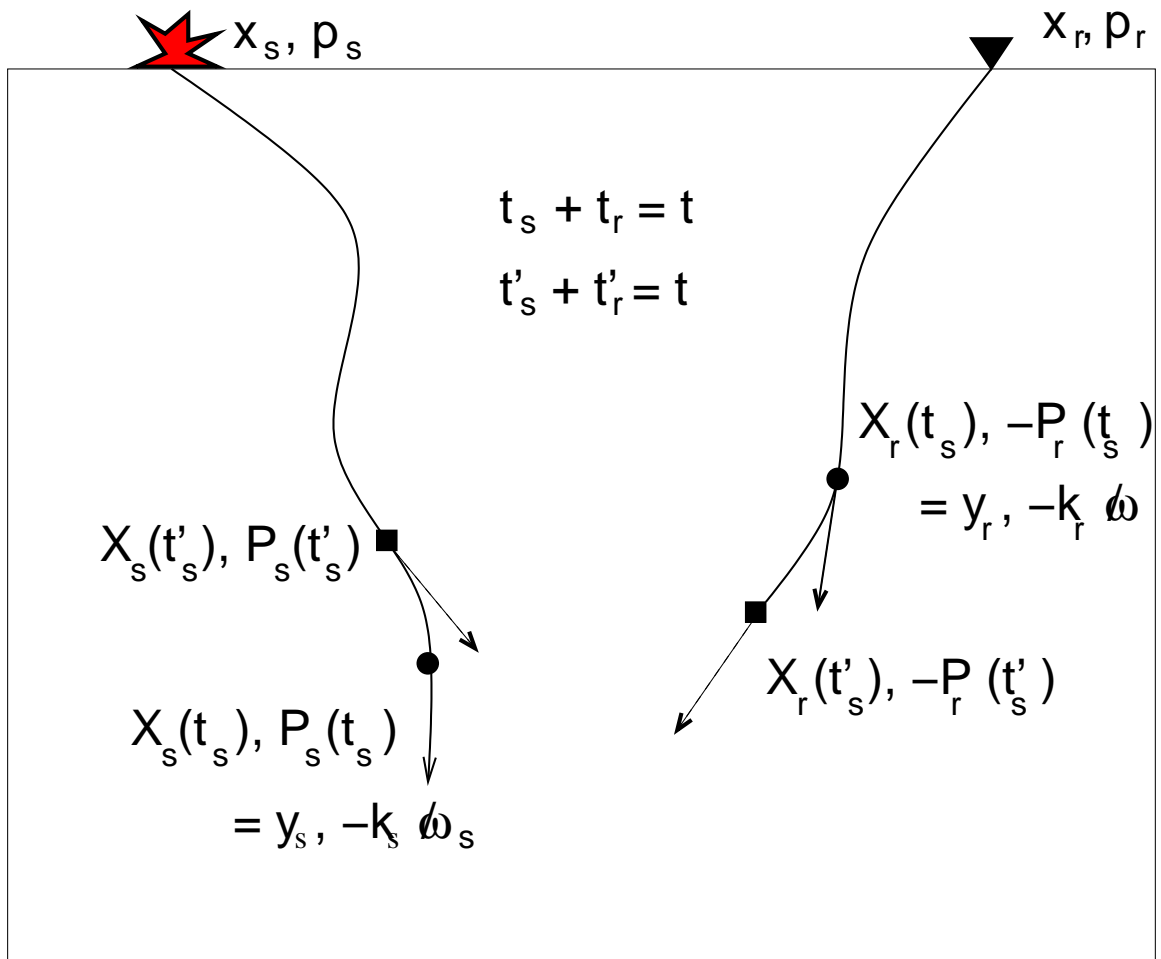


Figure number: 2

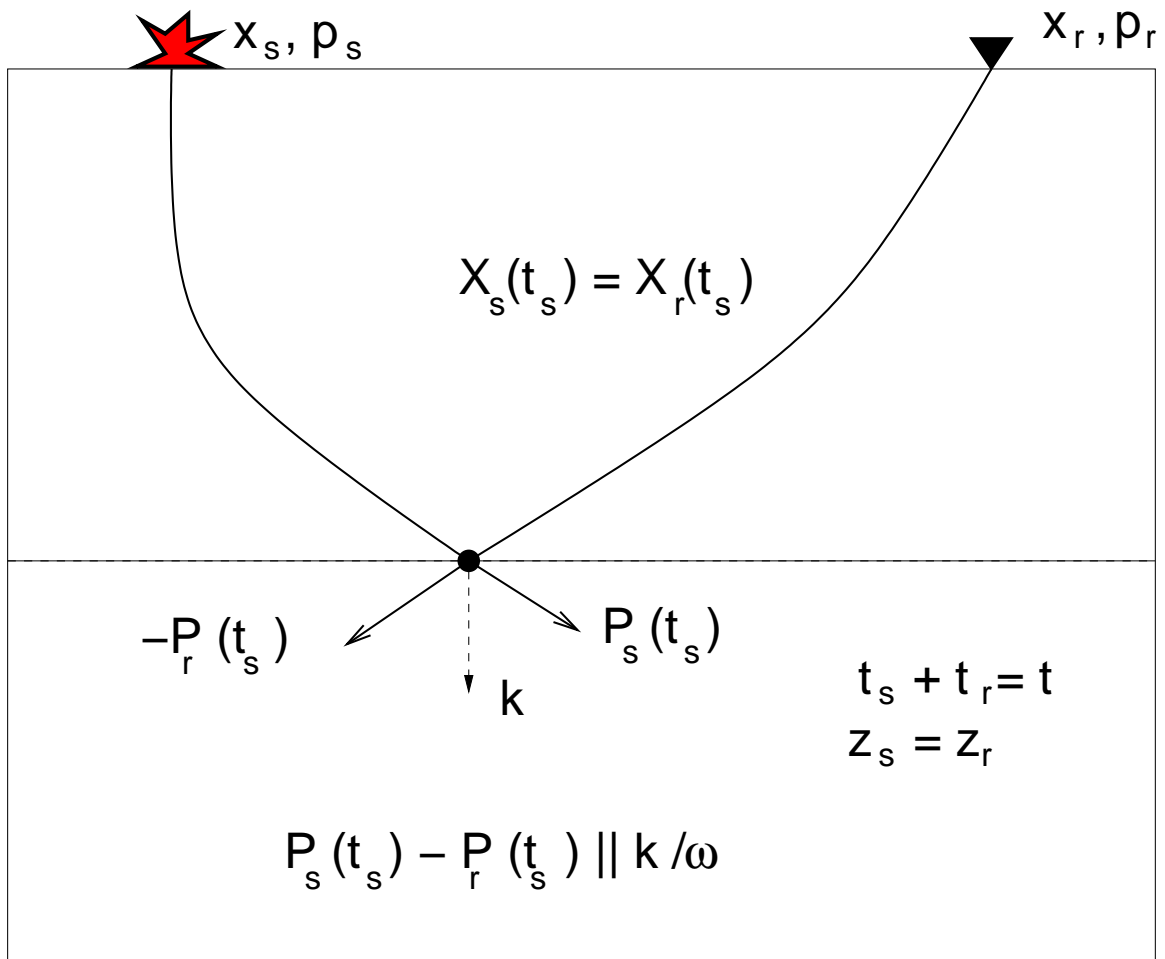


Figure number: 3

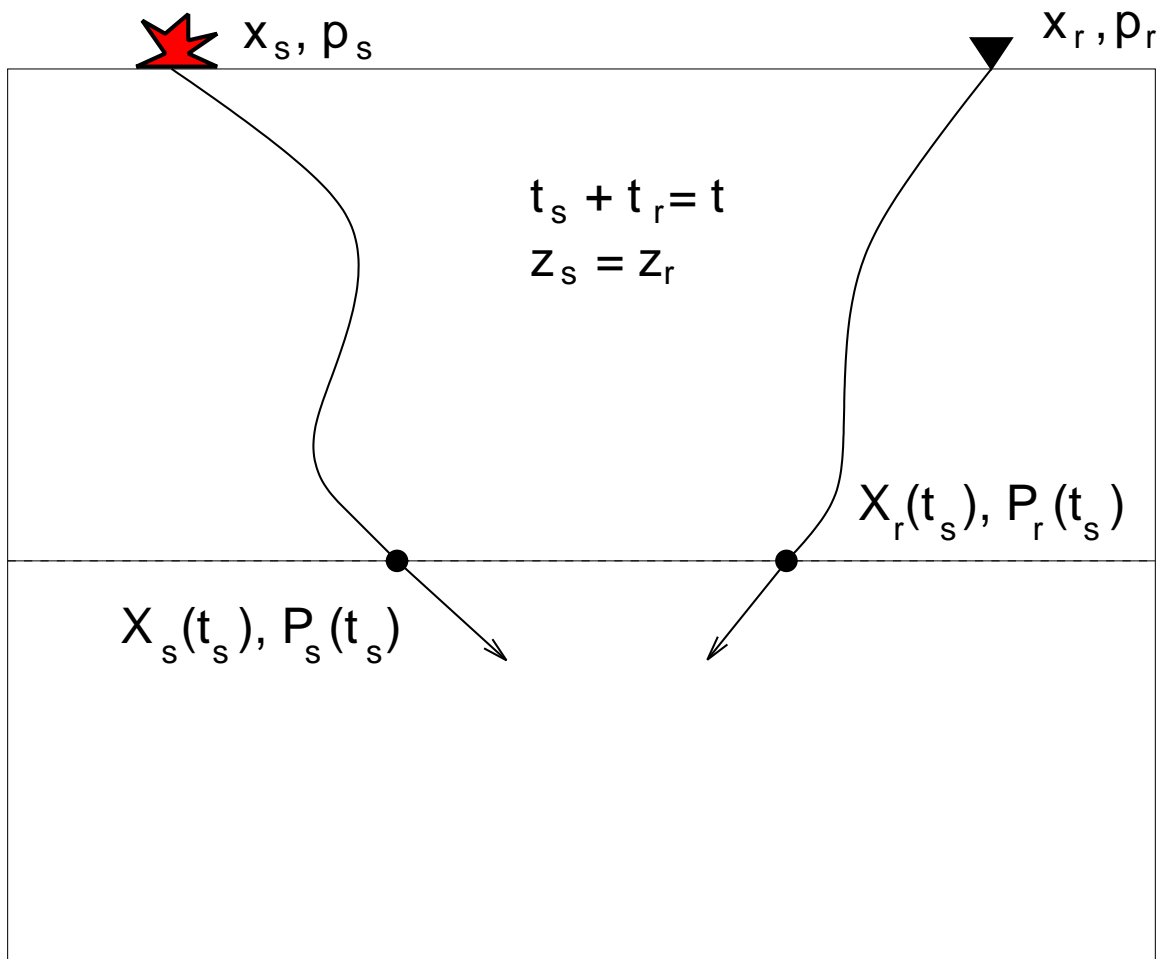


Figure number: 4

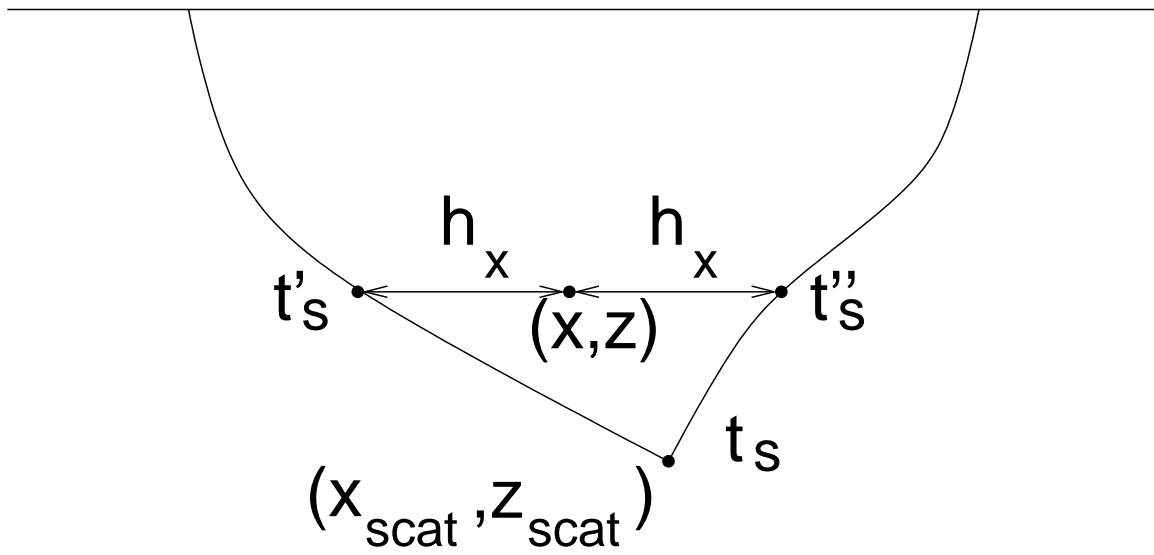


Figure number: 5

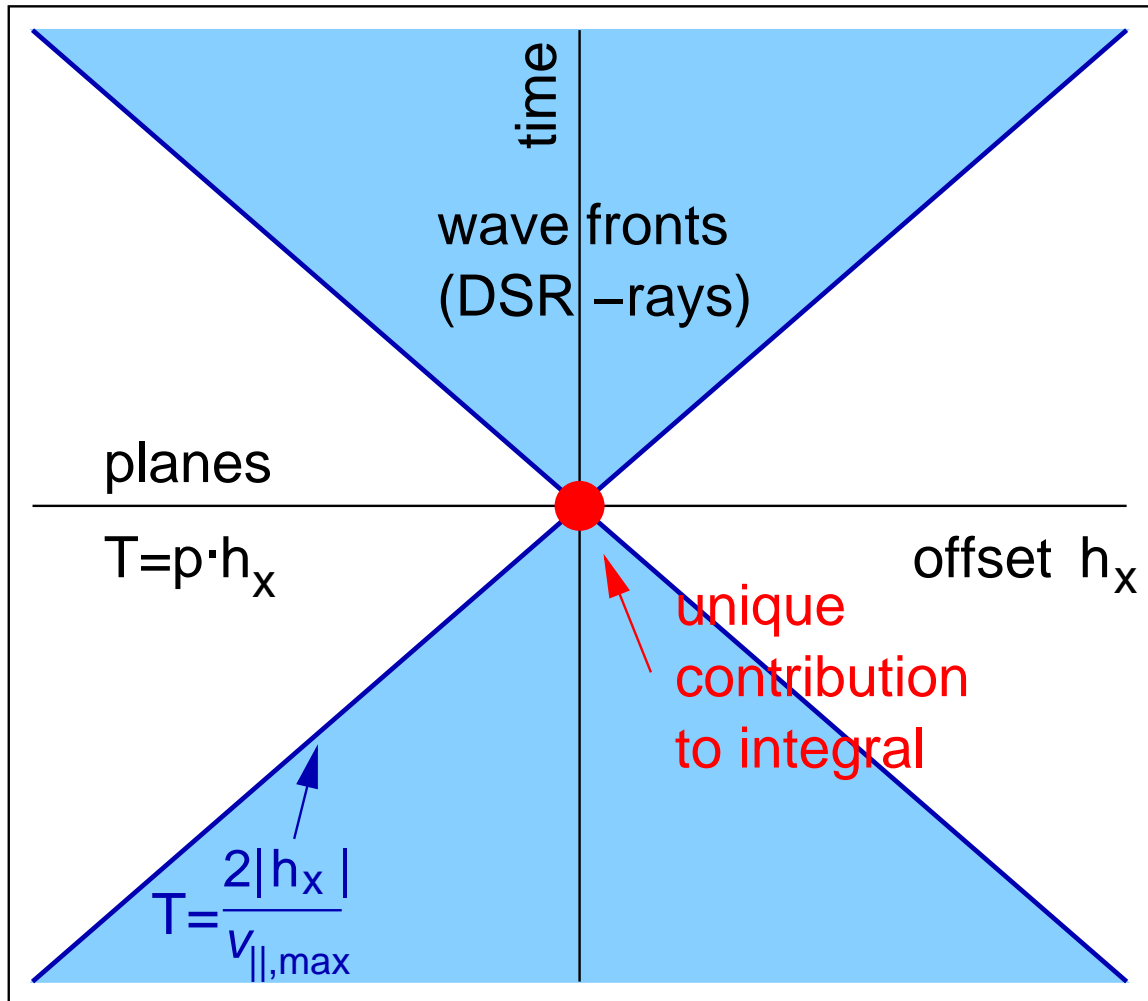


Figure number: 6

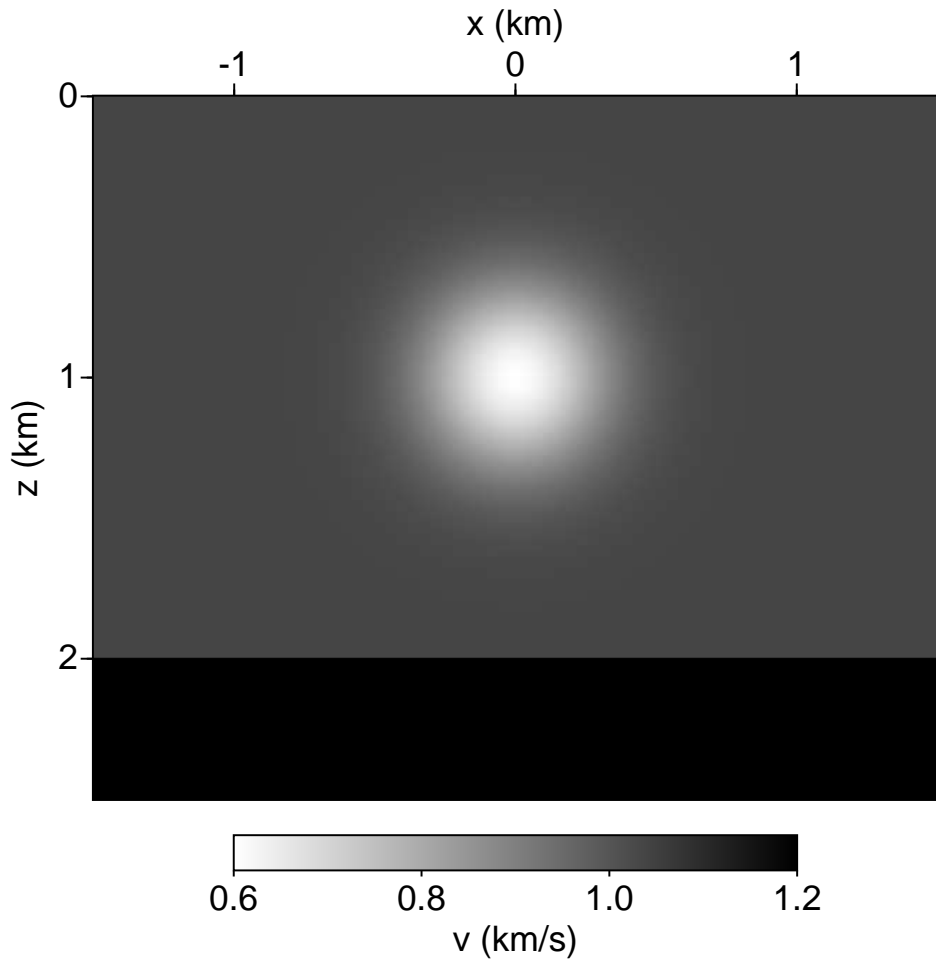


Figure number: 7

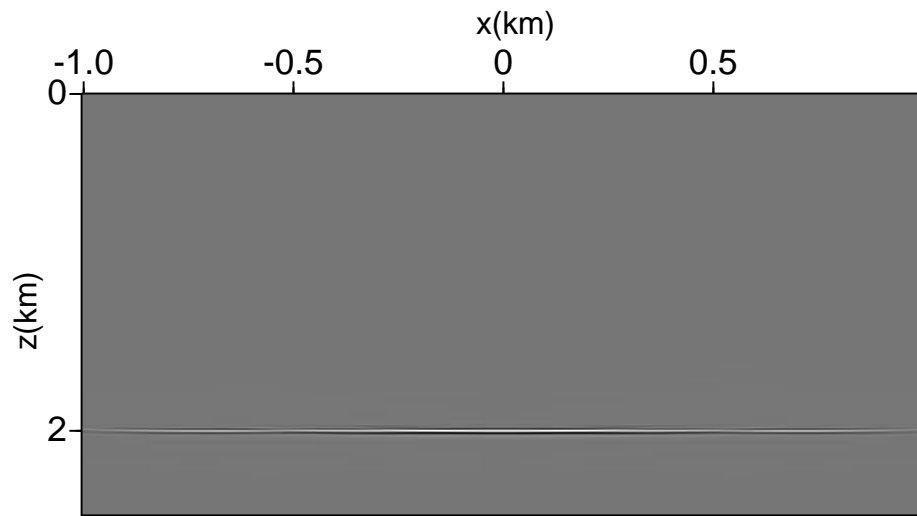


Figure number: 8

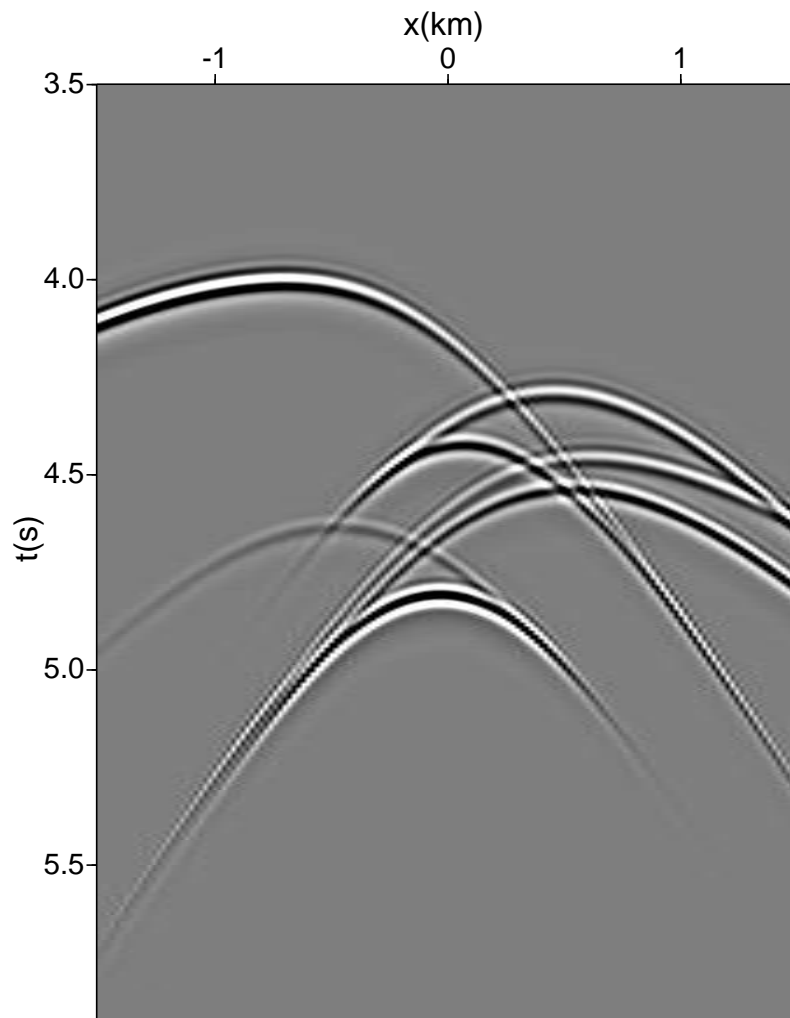


Figure number: 9

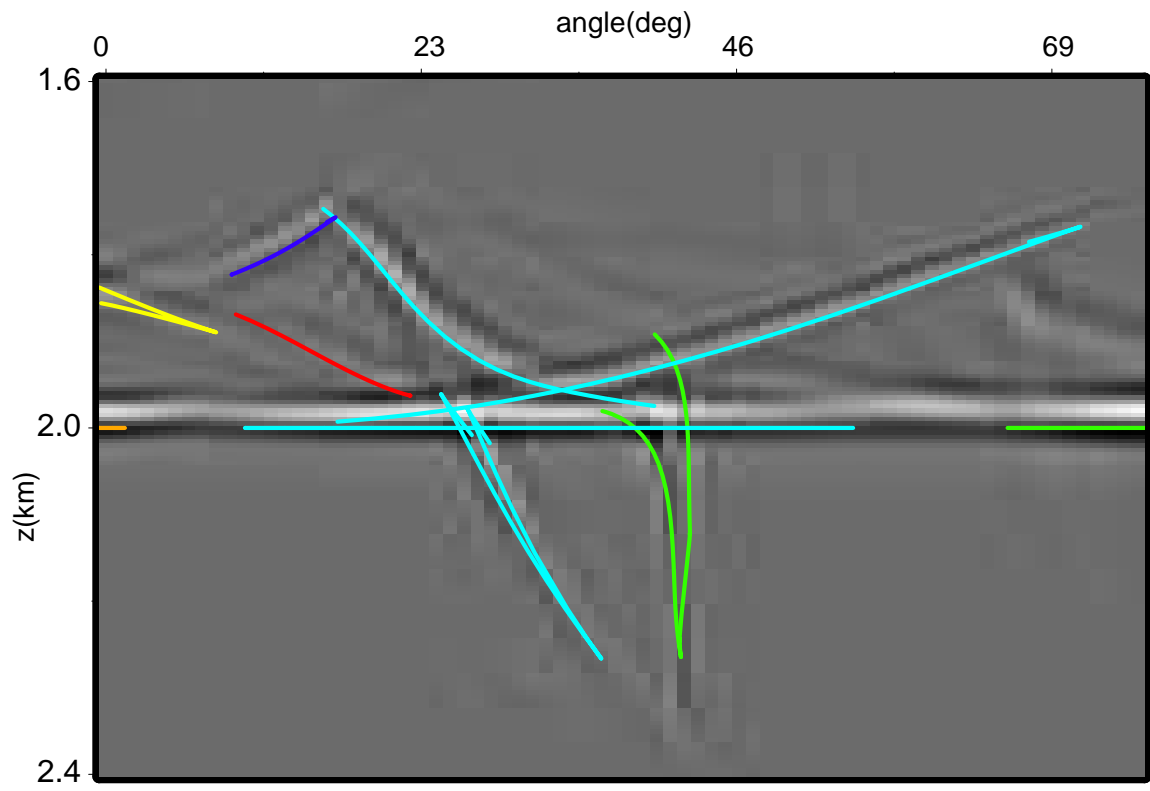


Figure number: 10

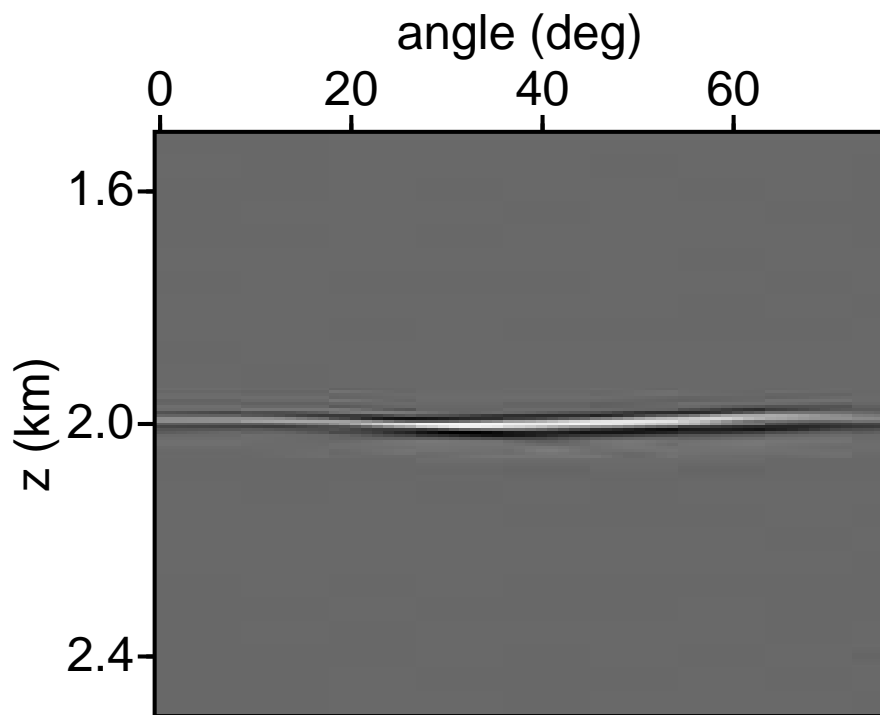


Figure number: 11

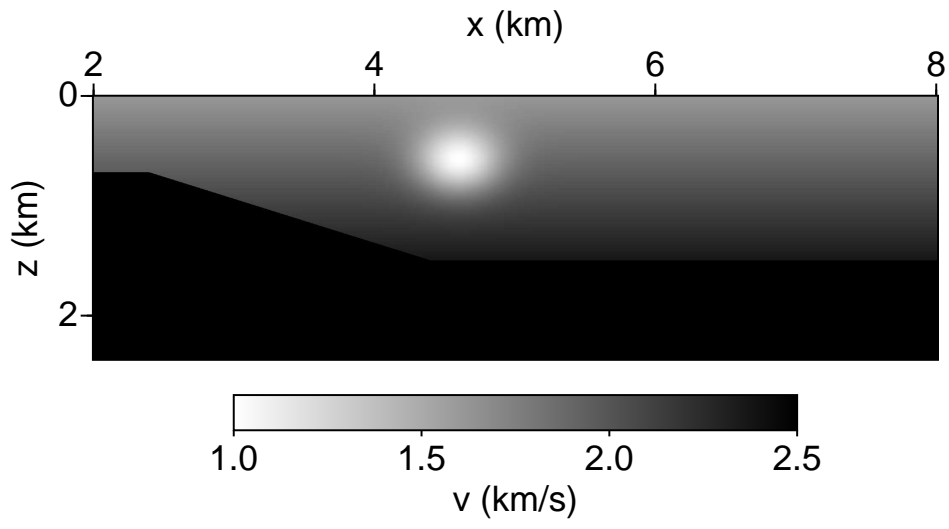


Figure number: 12

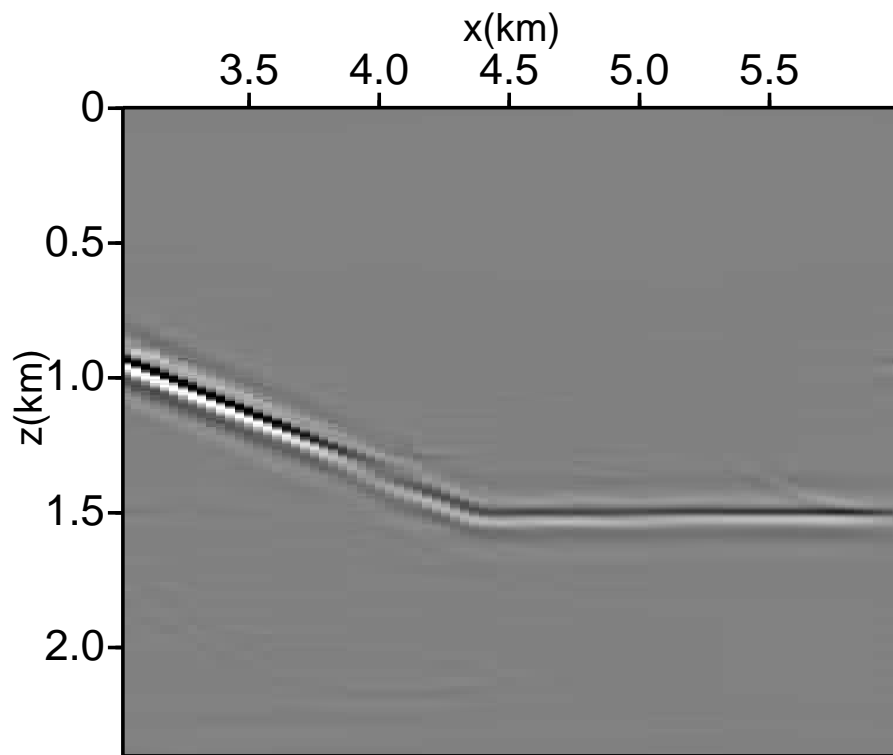


Figure number: 13

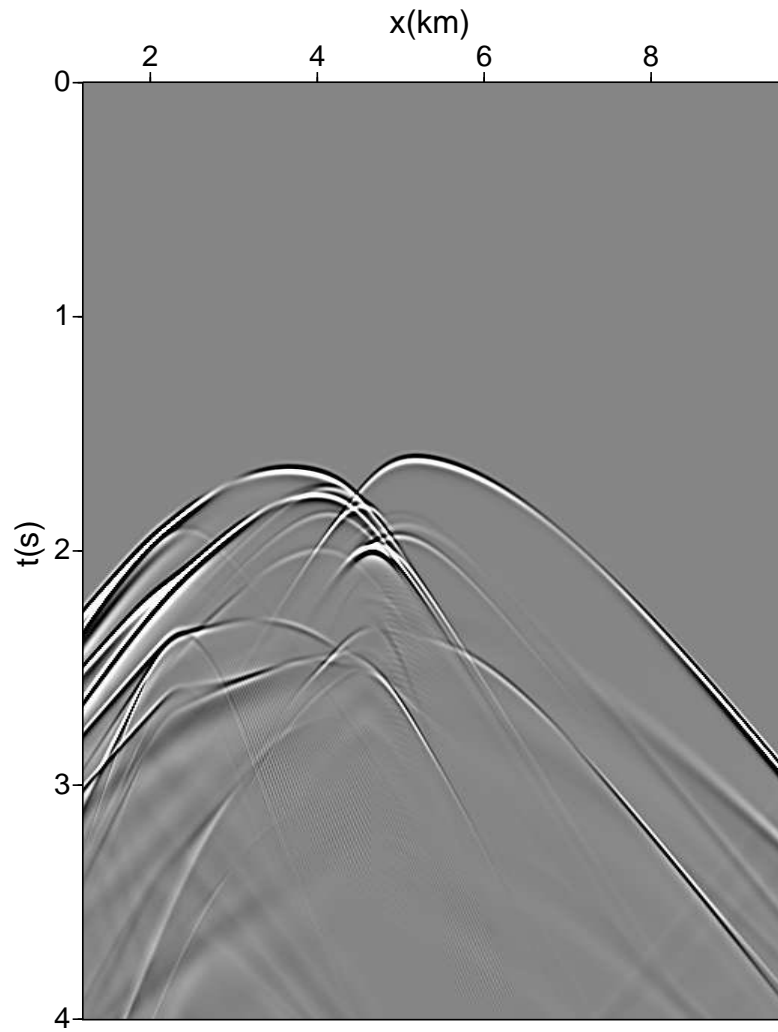


Figure number: 14

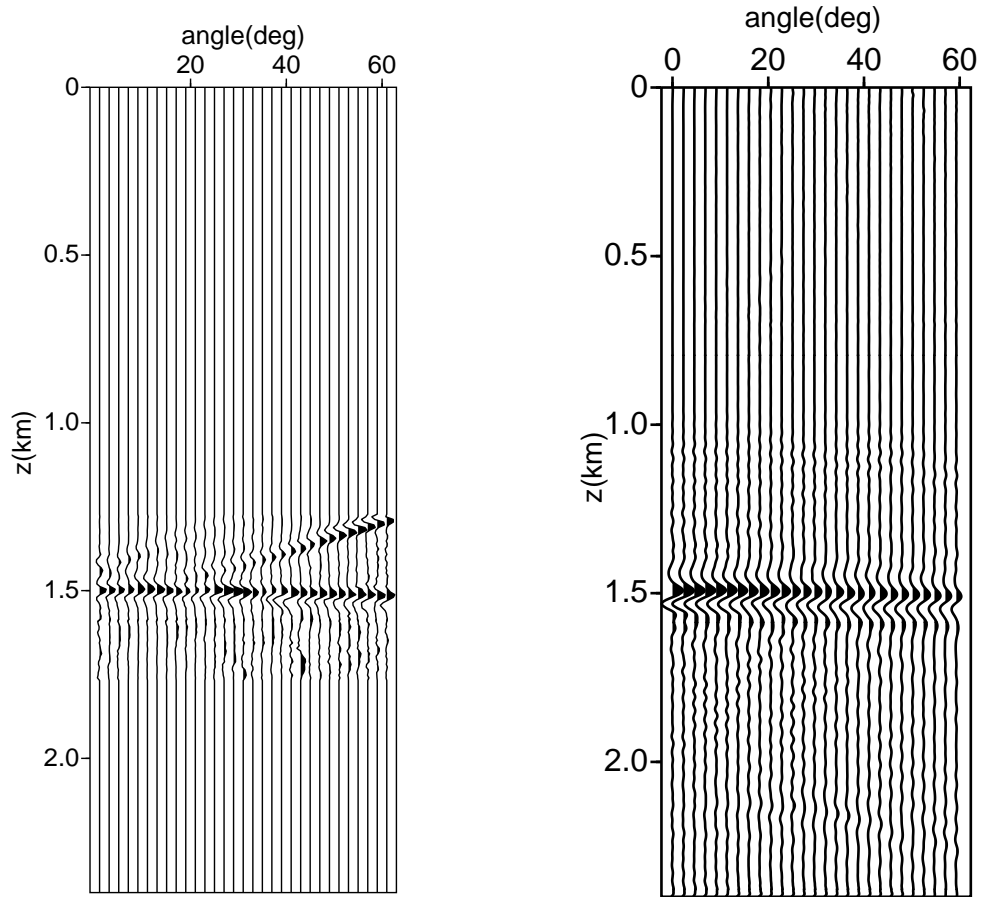


Figure number: 15

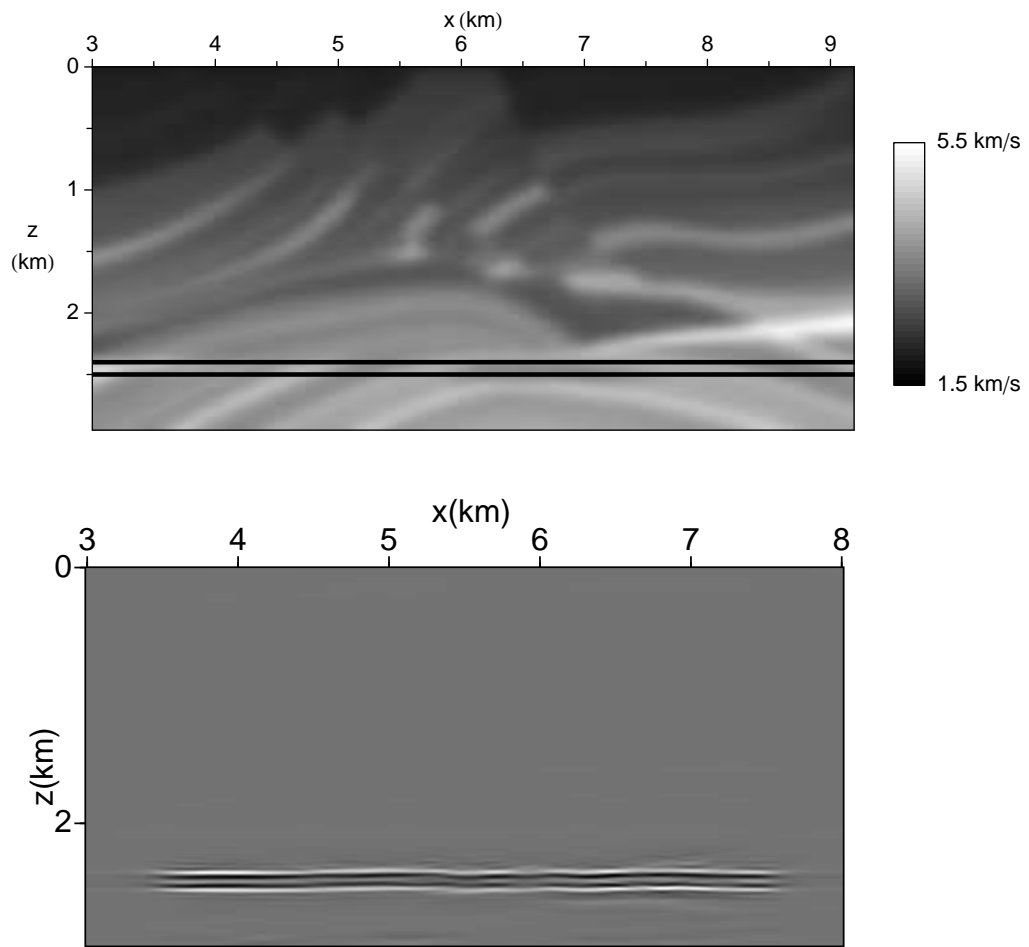


Figure number: 16

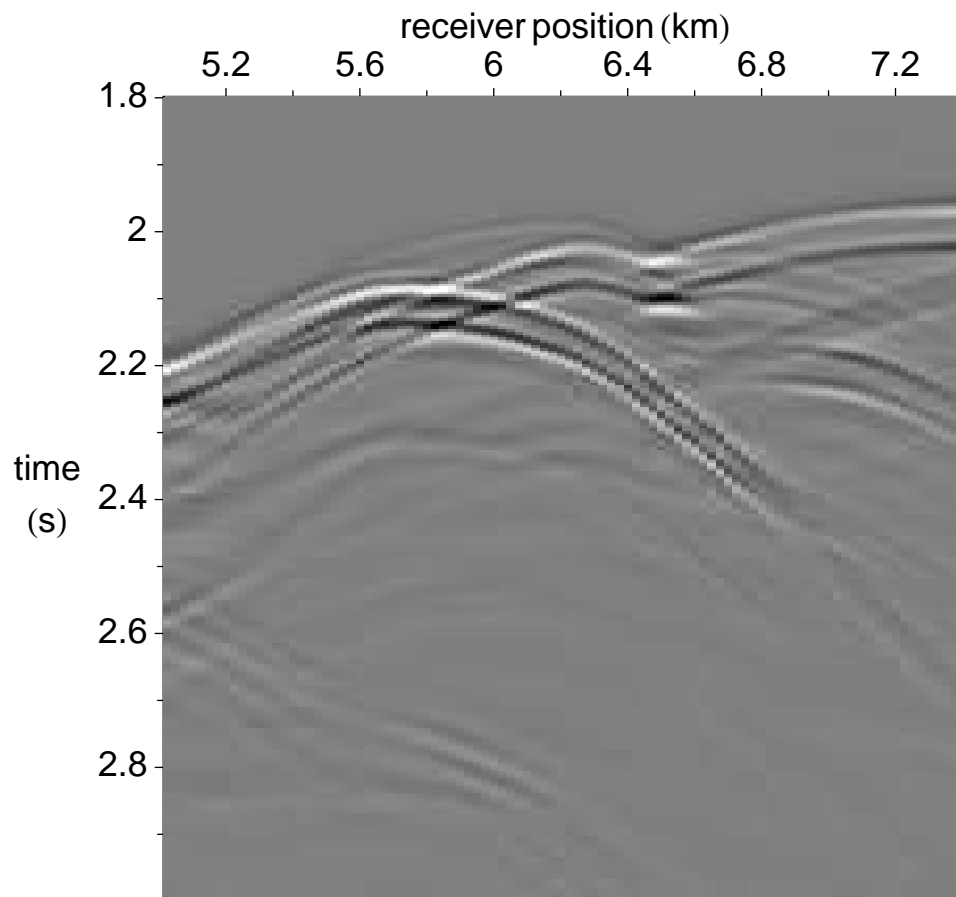


Figure number: 17

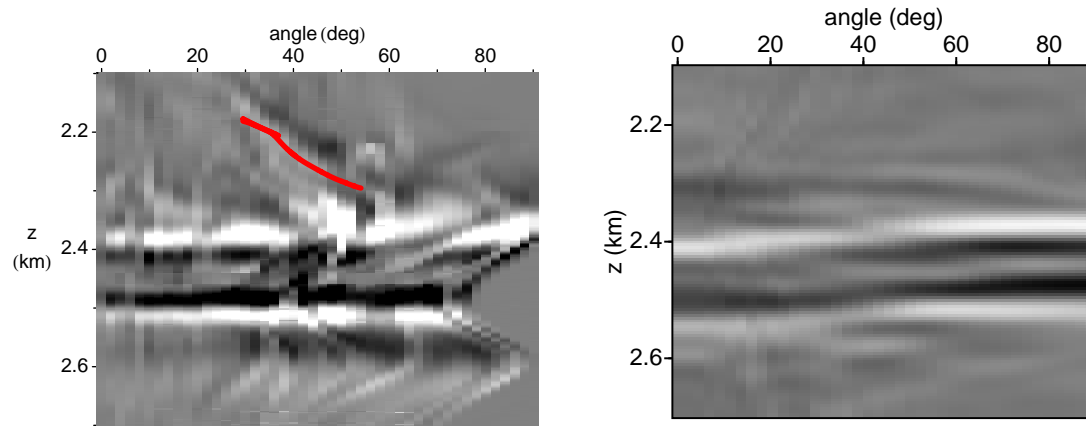


FIG. 1. Ray theoretic relation between data event and double reflector.

FIG. 2. Ray theoretic relation between data event and physical (single) reflector.

FIG. 3. Ray geometry for double reflector with horizontal offset only

FIG. 4. Ray geometry for offset-time angle gather construction.

FIG. 5. Cone in phase space for energy admitted to angle gather construction.

FIG. 6. Lens velocity model over flat reflector.

FIG. 7. DSR image of data lens velocity model, flat reflector.

FIG. 8. Lens model, shot record at shot location  $-500$  m.

FIG. 9. Lens model, common image point gather obtained with the Kirchhoff angle transform at  $x_m = 300$  m.

FIG. 10. Lens model, common image point gather obtained with the wave-equation angle transform (right) at  $x_m = 300$  m.

FIG. 11. Valhall velocity model.

FIG. 12. Valhall DSR image.

FIG. 13. Valhall lens model, shot record at shot location 4884 m.

FIG. 14. Valhall lens model, common image point gathers obtained with the Kirchhoff angle transform (left) and the wave-equation angle transform (right) at 4680 m.

FIG. 15. Marmousi derived model (top) and DSR image (bottom).

FIG. 16. Marmousi derived model, shot record at shot location 7500 m.

FIG. 17. Marmousi derived model, common image point gathers obtained with the Kirchhoff angle transform (left) and the wave-equation angle transform (right) at 6200 m.